FOREWORD

The research work described in this report was performed by the Bell Aerosystems Company, Buffalo, New York for the Flight Dynamics Laboratory Research and Technology Division, Wright Patterson Air Force Base, Ohio. The work was accomplished under Contract No. AF33(657)-7486, Project No. 8219, Task No. 821901 and entitled "Nonlinear Thermoelastic Effects on Hypersonic Stability and Control". Mr. H. M. Davis and J. E. Jenkins have been the Air Force Project Officers since the initiation of the program in November 1961. The study program was carried out by the Vehicle Structures Department of Bell Aerosystems Company under the technical direction of Mr. V. W. Donato until July 1962. Since then, Mr. J. R. Batt has been Technical Director.

Results of this program are being presented in a two-part report of which this is Part II. Part I presents a development of aerodynamic influence coefficients using an existing hypersonic aerodynamic theory. The results of a feasibility study employing Moire' fringe techniques to measure the angular displacements of practical wing structures are given under separate cover in FDL-TDR-64-42.

The authors wish to express their appreciation to Mr. E. J. Morris for his efforts in connection with the experimental phase of the study, to Miss M. Ostanski, and Mr. T. Hendricks for the coding of computer programs described herein, and to Mr. W. Luberacki for his many contributions to all phases of the study.

The digital computer FORTRAN program described in this report is available to eligible recipients from the Control Criteria Branch, Flight Control Division, A.F. Flight Dynamics Laboratory, Wright-Patterson A.F.B., Ohio, 45433.

ABSTRACT

An analytical method has been developed for the analysis of static aerothermoelastic behavior in the presence of nonlinear aerodynamic loads and geometrically nonlinear structural behavior. The method has been programmed for the IBM 7090 digital computer using FORTRAN coding techniques. A system for the experimental determination of static aerothermoelastic response of nonuniformly heated structures to loadings which are a nonlinear function of wing surface slopes has been developed. Results of this experimental program are presented and compared with theoretical predictions.

This technical documentary report has been reviewed and is approved.

C. R. Bryan
for W. A. SLOAN, Jr.
Colonel, USAF
Chief, Flight Control Division
AF Flight Dynamics Laboratory

TABLE OF CONTENTS

CONTENTS (CONT)

ILLUSTRATIONS

TABLES

SYMBOLS

b	wing span
c	wing chord
$\bar{c}$	wing average chord
k	element stiffness coefficient
$\frac{pb}{2V}$	helix angle made by wing tip during a rolling maneuver
p	angular rolling velocity
q	dynamic pressure
q_D	divergence dynamic pressure
u,v,w	displacements in the x, y, and z directions respectively
y^*	nondimensional spanwise coordinate
x,y,z	rectangular coordinates
C_L	lift coefficient
C_{L_α}	lift curve slope
E	modulus of elasticity
F	node point forces
K	stiffness coefficient in force-displacement equations for the complete structure
M	bending moment
M_∞	free stream Mach number
P	applied load
$Q_0, Q_1 \ldots Q_n$	aerodynamic influence coefficients
R	assigned reference point areas
α	equilibrium angle of attack
α_g	geometric or rigid angle of attack
α_s	streamwise angles produced by elastic deformation
δ	displacement influence coefficient
$\frac{\Delta p}{q}$	nondimensional lifting pressure
Δ	node point displacement
ν	Poisson's ratio
σ_t	spanwise thermal stress
Φ	loss of torsional stiffness parameter (see Equation (3.3))
η	incremental stiffness influence coefficient

SECTION 1.0

INTRODUCTION

Hypersonic flight conditions produce significant nonlinearities in aerodynamic behavior and, due to kinetic heating, are likely to introduce a nonlinear structural response. In the area of static aeroelasticity, (and its effects on stability and control derivatives) where aerodynamic and structural response interact and must be dealt with in combination, the analytical determination of the influence of such combined nonlinear behavior on the various static aeroelastic parameters has been a heretofore unaccomplished objective. In fact, although the nonlinear form of hypersonic aerodynamic operators has been well established through both theory and experiment on rigid airfoils, [1,2] and the structural nonlinearities of interest have been similarly established, [3-6] there is neither analytical nor experimental evidence pertaining to situations where such nonlinear phenomena act in combination.

Because of these deficiencies in a technology that may assume great importance in contemplated aerospace projects, a study was undertaken with the following objectives:

(1) Development of a method for obtaining hypersonic aerodynamic influence coefficients which extends the region of application of the methods of Reference 1.

(2) The formulation of governing mathematical relationships and development of a method and related computer program for the analysis of nonlinear static aeroelastic behavior.

(3) Development of a technique for the simulation and measurement of static aeroelastic behavior in the presence of aerodynamic and structural nonlinearities and elevated temperatures, as well as the actual measurement of data under such conditions.

(4) Analyses and comparisons with the test data obtained through objective (3).

Manuscript released by the authors January 1964 for publication as an FDL Technical Documentary Report.

(5) An exploratory examination of an experimental technique for measuring the slopes over the entire "field" of a deformed lifting surface.

Objectives (2) - (4) are discussed in the present report; work performed in accomplishment of objectives (1) and (5) is described in References 7 and 8, respectively.

In the analysis of practical airframes, the governing mathematical relationships of static aeroelastic interaction are usually written in matrix algebra. The aerodynamic input to these equations is a set of operators called aerodynamic influence coefficient matrices, which relate the nondimensional lifting pressure $\left\{\frac{\Delta p}{q}\right\}$ to the equilibrium angle of attack $\{\alpha\}$. In the subsonic and supersonic speed ranges a linear aerodynamic relation is obtained.

$$\left\{\frac{\Delta p}{q}\right\} = \left[Q\right]\left\{\alpha\right\} \tag{1.1}$$

Methods for obtaining such matrices are given in References 9 to 11. In the hypersonic speed range the aerodynamic equation may be of the following nonlinear form.

$$\left\{\frac{\Delta p}{q}\right\} = \left\lfloor Q_0 \right\rceil \left\{1\right\} + \left\lfloor Q_1 \right\rceil \left\{\alpha\right\} + \left\lfloor Q_2 \right\rceil \left\{\alpha^2\right\} \tag{1.2}$$

In inviscid hypersonic flow, the pressure at a reference point is a function of the angle of attack at only that point, resulting in the diagonal Q matrices shown in Equation (1.2). This point relationship between pressure and angle of attack does not exist in subsonic and supersonic flow; consequently, Q matrices for these flight regimes are nondiagonal.

A method for obtaining inviscid hypersonic aerodynamic influence coefficients was developed on a previous Air Force sponsored study program (Reference 1). The method, however, is restricted in its application. Thus, as part of the present study, a method for obtaining aerodynamic influence coefficients which extends the region of application of the method of Reference 1 has been developed. The results of this phase of the study are presented in Reference 7. The present report only briefly reviews the results presented in References 1 and 7.

The structural input to the static aeroelastic interaction equations is a set of structural influence coefficients $\left[\delta_{\alpha z}\right]$ which relate the angular elastic deformations (response) $\left\{\alpha_s\right\}$ to the lifting pressures. This relationship is written as

$$\left\{\alpha_s\right\} = q \left[\delta_{\alpha z}\right] \left\lfloor R \right\rfloor \left\{\frac{\Delta p}{q}\right\} \tag{1.3}$$

where $\left\lfloor R \right\rfloor$ is a diagonal matrix, each term of which is the amount of surface area assigned to each reference point, and q is the dynamic pressure. With regard to the evaluation of structural response, both "material property" (inelastic) and "geometric" nonlinearities may prove significant in the design of hypersonic vehicles. The present report is concerned only with geometric nonlinearities. Probably the simplest example of geometrically nonlinear behavior is provided by the transversely-loaded beam segment supported in the manner shown in Figure 1.1 below. The length of the neutral line under a transverse load is greater than in the unloaded state, requiring the existence of an axial ("midplane") load whose magnitude is proportional to the square of the slope α . The relationships between the transverse loads and the slopes will now involve the axial loads. Since the axial loads are a nonlinear function of the slopes the problem is not only nonlinear but also involves the coupling of the equations for axial and flexural behavior, respectively.

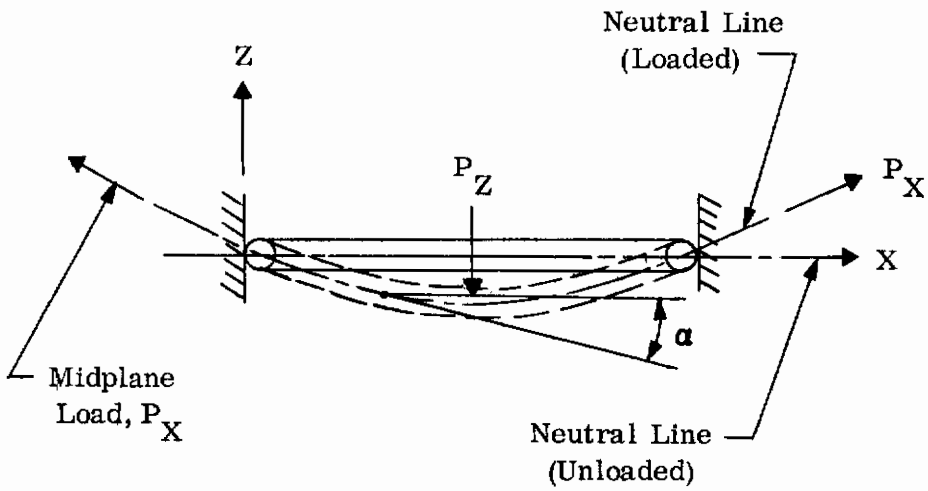

Figure 1.1. Beam Segment

Clearly, in a cantilever beam there are no effects of the above type. Hypersonic wings, however, cannot generally be represented as cantilevers (as lines) but are actually two-dimensional (surfaces). Such surfaces are influenced by the effects described above. These effects can prove significant for maximum displacements which are a multiple of the wing thickness. The multiple is a function of the wing geometric proportions and the material elastic properties, as well as other factors influencing stiffness (e.g., aerodynamic heating); it will be larger than 1.0 but cannot be defined with precision. The present report develops mathematical relationships which describe the above phenomena for the plate type wings. Previous studies (References 12-15) have resulted in methods for determining $\left[\delta_{\alpha z} \right]$ matrices for complex built-up wings and fuselages.

Difficulties arise in formulating and solving the aeroelastic interaction equations for hypersonic flight vehicles since the relations between lifting load and angle of attack are no longer linear, and because the structural relations between load and deformation (when considering large deflections) are also nonlinear. In an earlier study (Reference 16) efforts were restricted to using nonlinear aerodynamic inputs and linear structural inputs. Various numerical techniques were employed to obtain a solution for the equilibrium angle of attack. Section 2.0 of the present report extends the work of Reference 16 to include nonlinear structural inputs, while retaining nonlinear aerodynamic inputs, in the solution of the aeroelastic interaction equations. In addition, a digital computer program for the analysis of the subject phenomena is developed. This program, coded in FORTRAN, provides for the computation of the equilibrium angle of attack, flexible to rigid span loadings and lifting pressures, lift coefficients and other pertinent static aeroelastic parameters. Capabilities of the program include the computation of structural slope influence coefficients at certain $\left\{ \alpha \right\}$ iteration steps (Points B and C for example, Figure 2.1) and for nonlinear structural behavior. Nonlinear aerodynamic relationships are accounted for by providing either a quadratic, cubic or transcendental variation of lifting pressure with angle of attack. The FORTRAN program is designed so that analyses can be made which (a) account for nonlinear aerodynamics combined with linear structural response, or (b) account for nonlinear aerodynamics combined with nonlinear structural response. The program is available to eligible receipients upon request from the Air Force Project Officer (See Foreword).

The development of a technique for the simulation and measurement of wing static aeroelastic behavior in the presence of aerodynamic and structural nonlinearities and elevated temperatures is described in Section 3.0 of this report. The technique is based upon the point relationship existing between lifting pressure and angle of attack. Simulation of aerodynamic nonlinearities was accomplished by using certain electrical circuitry in conjunction with an accelerometer which measured local angular structural deformation. The use of an accelerometer to measure such deformation is unique; usually, optical methods of the type discussed in References 18 and 19 are utilized. Structural nonlinearities are simulated by providing the proper test inputs, such as elevated temperatures, specimen dimensions, material properties and external loadings which create large deflections.

Test results obtained from the above simulation technique are compared in Section 4.0 with theoretical predictions using the digital computer program developed in Section 2.0. Analyses are presented for nonlinear aerodynamic and linear structural behavior and nonlinear aerodynamic and nonlinear structural behavior for the test specimen used in the experimental program. Section 5.0 presents conclusions and recommendations for this portion of the study program.

SECTION 2.0
NONLINEAR STATIC AEROELASTIC SOLUTIONS

2.1 GENERAL

A method capable of predicting the static aerothermoelastic response of a lifting surface is described in this section. As formulated, the method accounts for both nonlinear aerodynamic and structural behavior and is consistent with the "field" approach, wherein the behavior of a lifting surface is represented by designated planform "reference" points. It is assumed that the surface being studied is a diverging type surface, i.e. it possesses a positive divergence dynamic pressure. The method, however, is completely general and is equally applicable to the analysis of a non-diverging type surface. The basis of the method was developed in Reference 16 under the title "Nonlinear Lifting Pressure Component Method", considering only aerodynamic nonlinearities. Here, this method is extended to include structural nonlinearities.

2.2 FORMULATION OF GOVERNING MATHEMATICAL RELATIONSHIPS

As noted previously, the field approach involves the representation of a lifting surface by numerous reference points where each reference point is assigned a portion of the surface area. The aerodynamic pressures and inertial forces on each assigned area are assumed to act as concentrated forces on the corresponding points. In the development of stability and control derivatives, for example, the aeroelastician will require knowledge of the equilibrium angles of attack $\left\{\alpha\right\}$ at the reference points. These angles can be considered to be composed of two parts; namely, the angles $\left\{\alpha_s\right\}$ produced by structural deformation, and the angles $\left\{\bar{\alpha}_g\right\}$ which are either built-in or arise from "fixed" sources. In certain instances, the effect of inertial forces can and should be included. Thus, the following expression for the equilibrium angle of attack results:

$$\left\{\alpha\right\} = \left\{\alpha_s\right\} + \left\{\bar{\alpha}_g\right\} \tag{2.1}$$

More precisely, $\left\{\bar{\alpha}_g\right\}$ is the sum of a number of angular components defined as follows:

$$\left\{\bar{\alpha}_g\right\} = \left\{\alpha_g\right\} + \left\{\alpha_T\right\} + \left\{\left(\frac{pb}{2V}\right)y^*\right\} + \left\{\delta_{Ref}\right\}^* \qquad (2.2)$$

$$\left\{\alpha_g\right\} = \alpha_{Ref}\left\{1\right\} + \alpha_{b_i}\left\{1\right\} + \left\{\alpha_{b_t}\right\}$$

where α_T = initial angular displacement due to temperature

$\frac{pb}{2V}$ = helix angle made by wing tip during a rolling maneuver

δ_{Ref} = control surface deflection angle.

α_{Ref} = angle between the aircraft reference axis and wind

α_{b_i} = angle between lifting surface reference axis and aircraft reference axis

α_{b_t} = rigid spanwise angle distribution due to built in twist.

$y^* = \frac{y}{\frac{b}{2}}$

It is assumed that a set of "structural influence coefficients" $\left[\delta\alpha_Z\right]$, relating the angular elastic deformations $\left\{\alpha_s\right\}$ to the pertinent applied loads $\left\{P_Z\right\}$, can be derived.** These relationships are written as

$$\left\{\alpha_s\right\} = \left[\delta\alpha_Z\right]\left\{P_Z\right\} \qquad (2.3)$$

Also, the applied loads $\left\{P_Z\right\}$ are related to the nondimensional lifting pressures $\left\{\frac{\Delta p}{q}\right\}$ as follows:

$$\left\{P_Z\right\} = q\left\lfloor R\right\rceil\left\{\frac{\Delta p}{q}\right\} \qquad (2.4)$$

The symbol $\lfloor\ \rceil$ denotes a diagonal matrix; i.e., each row contains a value on the main diagonal and zeros elsewhere. $\lfloor R\rceil$, as indicated, is a diagonal matrix; each term in $\lfloor R\rceil$ is the amount of surface area assigned to each reference point. A matrix, $\left[Q\right]$, of "aerodynamic influence coefficients", which relates the

---

*These definitions are in accordance with the method of Reference 16 pg 34 and 35 except that $\left\{\bar{\alpha}_g\right\}$ is defined somewhat differently in this report due to the introduction of structural nonlinearities.

**See footnote page 27.

reference point equilibrium angles of attack $\{\alpha\}$ to the nondimensional lifting pressures, can be constructed.

Thus, $$\left\{\frac{\Delta p}{q}\right\} = \left[Q\right] \{\alpha\} . \tag{2.5}$$

Combining Equations (2.1) through (2.5) results in

$$\{\alpha\} = q \left[\delta_{\alpha Z}\right] \lfloor R \rceil \left[Q\right] \{\alpha\} + \{\bar{\alpha}_g\} \tag{2.6}$$

Under linear circumstances, Equation (2.6) can be solved to yield

$$\{\alpha\} = \left[\lfloor 1 \rceil - q \left[\delta_{\alpha Z}\right] \lfloor R \rceil \left[Q\right]\right]^{-1} \{\bar{\alpha}_g\} \tag{2.7}$$

where $\lfloor 1 \rceil$ is the unit matrix.

This report is concerned with circumstances where the aerodynamic behavior, as represented by $\left[Q\right]$, is an explicit nonlinear function of $\{\alpha\}$ and the structural behavior, as represented by $\left[\delta_{\alpha Z}\right]$, is an implicit nonlinear function of $\{\alpha\}$. These matters will now be given more detailed consideration.

Aerodynamic influence coefficients for hypersonic flight are comprehensively reviewed in Reference 1, only a brief description of these coefficients is given here. Such coefficients may assume several different forms, depending on the aerodynamic configuration and theory being used, but are in each case functions of α and governed by the premise that the aerodynamic load at a point is a function of the angle of attack at only that point. In consequence of this latter premise, the aerodynamic influence coefficient matrix on the right side of Equation (2.5) is of diagonal form; i.e., $\lfloor Q \rceil$.

To exemplify the form of hypersonic aerodynamic influence coefficients, consider the lifting pressure relationship derived from the theory of Reference 20 where, at reference point i:

$$\left(\frac{\Delta p}{q}\right)_i = Q_{0_i} + Q_{1_i} \alpha_i + Q_{2_i} \alpha_i^2 + Q_{3_i} \alpha_i^3 \tag{2.8}$$

Or using the theory of Reference 21 for blunted airfoils

$$\left(\frac{\Delta p}{q}\right)_i = Q_{a_i} \sin Q_{b_i} \alpha_i \tag{2.9}$$

The coefficients of α_i are presented graphically in Reference 1 as a function of Mach number and airfoil thickness ratio for a variety of cross-sectional shapes.

These aerodynamic relationships can be written in a more general form as

$$\left\{\frac{\Delta p}{q}\right\} = \left[\left\lfloor \frac{Q_o}{\alpha} \right\rceil + \left\lfloor Q_1 \right\rceil + \left\lfloor \frac{Q_n}{\alpha} \right\rceil\right]\{\alpha\} \tag{2.10}$$

where $$\left\lfloor Q_n \right\rceil = \left\lfloor Q_2 \right\rceil \left\lfloor \alpha^2 \right\rceil + \left\lfloor Q_3 \right\rceil \left\lfloor \alpha^3 \right\rceil \tag{2.11}$$

or $$\left\lfloor Q_n \right\rceil = \left\lfloor Q_a \right\rceil \left\lfloor \sin Q_b \alpha \right\rceil - \left\lfloor Q_o \right\rceil \{1\} - \left\lfloor Q_1 \right\rceil \left\lfloor \alpha \right\rceil \tag{2.12}$$

Note that this expression differs from the convential form, Equation (2.5), not only in the nonlinear terms such as $Q_{2_i} \alpha_i^2$ but also in the presence of the constant term $Q_{o_i} = \left(\frac{\Delta p}{q}\right)_{o_i}$. This term arises due to airfoil camber or thickness, and is of direct use in the aeroelastic simulation scheme discussed in Section 3.0.

Substitution of Equation (2.10) into Equation (2.4) yields

$$\{P_Z\} = q\left\lfloor R \right\rceil \left\{\left(\frac{\Delta p}{q}\right)_o\right\} + q\left\lfloor R \right\rceil \left[\left\lfloor Q_1 \right\rceil + \left\lfloor \frac{Q_n}{\alpha} \right\rceil\right]\{\alpha\} \tag{2.13}$$

or $$\{P_Z\} = \{P_{Z_o}\} + \left[\left\lfloor \bar{Q}_1 \right\rceil + \left\lfloor \frac{\bar{Q}_n}{\alpha} \right\rceil\right]\{\alpha\} \tag{2.14}$$

where by definition

$$\{P_{Z_o}\} = q\left\lfloor R \right\rceil \left\{\left(\frac{\Delta p}{q}\right)_o\right\} = q\left\lfloor R \right\rceil \left\lfloor Q_o \right\rceil \{1\},$$

$$\left\lfloor \bar{Q}_1 \right\rceil = q\left\lfloor R \right\rceil \left\lfloor Q_1 \right\rceil \quad \text{and} \quad \left\lfloor \bar{Q}_n \right\rfloor = q\left\lfloor R \right\rceil \left\lfloor Q_n \right\rceil$$

Next substituting Equation (2.14) into Equation (2.3) and that in turn into Equation (2.1), yields

$$\{\alpha\} = \left[\delta_{\alpha Z}\right]\{P_{Z_o}\} + \left[\delta_{\alpha Z}\right]\left[\left\lfloor \bar{Q}_1 \right\rceil + \left\lfloor \frac{\bar{Q}_n}{\alpha} \right\rceil\right]\{\alpha\} + \{\bar{\alpha}_g\} \tag{2.15}$$

The matrix product $\left[\delta_{\alpha Z}\right]\left\{P_{Z_o}\right\}$ (on the right-hand side of Equation (2.15)), leads to a set of "effective" geometric angles of attack $\left\{\alpha_{g_o}\right\}$ since for $\left\{\alpha\right\} = \left\{\bar{\alpha}_g\right\} = \left\{0\right\}$, the known initial loads $\left\{P_{Z_o}\right\}$ produce a set of known initial angles. Use is made of this fact in the aeroelastic simulation technique.

If an attempt is made to solve Equation (2.15) for $\left\{\alpha\right\}$ in the same manner as the linear solution, Equation (2.7) was obtained, the following result is indicated:

$$\left\{\alpha\right\} = \left[\left\lfloor 1 \right\rceil - \left[\delta_{\alpha Z}\right]\left\lfloor \left\lfloor \bar{Q}_1 \right\rceil + \left\lfloor \frac{\bar{Q}_n}{\alpha} \right\rceil \right\rfloor\right]^{-1} \left\{\left\{\bar{\alpha}_g\right\} + \left\{\alpha_{g_o}\right\}\right\} \tag{2.16}$$

where $\left\{\alpha_{g_o}\right\} = \left[\delta_{\alpha Z}\right]\left\{P_{Z_o}\right\}$.

It is not actually possible to achieve this result in a direct manner, however, since the matrix to be inverted contains the as yet unknown set of α's; furthermore, $\left[\delta_{\alpha Z}\right]$ is a function of $\left\{\alpha\right\}$. To solve Equation (2.16) numerically it is necessary to use iterative or other indirect techniques. This approach is discussed next, and an experimental means of solving Equation (2.16) is presented in Section 3.0. A discussion of the structural nonlinearities attendent with $\left[\delta_{\alpha Z}\right]$ are presented in Section 2.4.

2.3 METHOD OF SOLUTION

The basis of the method of solution was developed in Reference 16 under the title "Nonlinear Lifting Pressure Component Method." This method is extended to include nonlinear structural response and consists of an iteration technique to obtain a solution for the equilibrium angle of attack. A description of the method follows.

Equation (2.15) is rewritten as

$$\left\{\alpha\right\} = \left\{\bar{\alpha}_g\right\} + q\left[\delta_{\alpha Z}\right]\left\lfloor R \right\rceil \left\lfloor \left\lfloor \frac{Q_o}{\alpha} \right\rceil + \left\lfloor Q_1 \right\rceil + \left\lfloor \frac{Q_n}{\alpha} \right\rceil \right\rfloor \left\{\alpha\right\} \tag{2.17}$$

Let

$$\left[\Gamma\right] = \left[\delta_{\alpha Z}\right]\left\lfloor R \right\rceil \left\lfloor \left\lfloor \frac{Q_o}{\alpha} \right\rceil + \left\lfloor Q_1 \right\rceil + \left\lfloor \frac{Q_n}{\alpha} \right\rceil \right\rfloor \tag{2.18}$$

Then Equation (2.17) may be rewritten as

$$\left\{ \alpha \right\} = \left[\lfloor 1 \rceil - q \left[\Gamma \right] \right]^{-1} \left\{ \bar{\alpha}_g \right\} \tag{2.19}$$

which is of the same for as Equation (2.7) except that $\left[\Gamma \right]$ is a function of the unknown $\left\{ \alpha \right\}$. A solution for $\left\{ \alpha \right\}$ can be obtained from Equation (2.19) by an iterative process, wherein each iteration requires computing an inverse matrix. This is avoided by expanding the inverse matrix in a power series as

$$\left\{ \alpha \right\} = \left[\lfloor 1 \rceil + q \left[\Gamma \right] + q^2 \left[\Gamma \right]^2 + q^3 \left[\Gamma \right]^3 + \ldots + q^m \left[\Gamma \right]^m \right] \left\{ \bar{\alpha}_g \right\} + \left\{ R_e \right\}^* \tag{2.20}$$

where $\left\{ R_e \right\}$ is a set of remainder terms.

A solution can be obtained using Equation (2.20) by setting the remainder terms equal to zero and iterating the remaining expression. However, better convergence characteristics are obtained if the remainder term is included. As shown in Reference 16 pg 73, the remainder term can be easily determined resulting in the following forms of Equation (2.20).

$$\left\{ \alpha \right\} = \left\{ \bar{\alpha}_g \right\} + q \left[\Gamma \right] \left\{ \alpha \right\} \tag{2.21}$$

$$\left\{ \alpha \right\} = \left[\lfloor 1 \rceil + q \left[\Gamma \right] \right] \left\{ \bar{\alpha}_g \right\} + q^2 \left[\Gamma \right]^2 \left\{ \alpha \right\} \tag{2.22}$$

$$\left\{ \alpha \right\} = \left[\lfloor 1 \rceil + q \left[\Gamma \right] + q^2 \left[\Gamma \right]^2 \right] \left\{ \bar{\alpha}_g \right\} + q^3 \left[\Gamma \right]^3 \left\{ \alpha \right\} \tag{2.23}$$

$$\left\{ \alpha \right\} = \left[\lfloor 1 \rceil + q \left[\Gamma \right] + q^2 \left[\Gamma \right]^2 + \ldots + q^m \left[\Gamma \right]^m \right] \left\{ \bar{\alpha}_g \right\} + q^{m+1} \left[\Gamma \right]^{m+1} \left\{ \alpha \right\} \tag{2.24}$$

Each of the above equations is an exact representation of equilibrium conditions as defined by Equation (2.19) since no assumptions have been made in the derivation of Equations (2.21) to (2.24). Consequently, the same solution (within limits of numerical iterative techniques) may be obtained using any one of Equations (2.24) in accordance with an iterative process. Either Equation (2.19) or one of Equations (2.24)

---

*For this matrix power series to converge, the absolute value of the largest eigenvalue of $\left[\Gamma \right]$ must be less than 1. See Reference 22, page 317.

may be used as a basis for an iterative solution for the equilibrium angle of attack. In the interest of economizing on computation time it is usually preferable to use one of Equations (2.24). However, it should be recognized that better convergence properties are associated with use of Equation (2.19) in an iterative solution than with Equations (2.24).

The iterative process will be illustrated with the use of Equation (2.22) and Figure 2.1. This figure graphically portrays the steps followed in obtaining a solution for the equilibrium angle of attack. The heavy solid curve represents the nonlinear relationship between lifting pressure and angle of attack. The solid straight lines represent the linear relationship between angle of attack and structural response. Thus, the equilibrium state is given by the intersection of these two curves. The dashed line, proceeding from point A to point B, for example, represents an iteration path. The solution proceeds as follows:

Steps	Equation
(1) Assume an initial set of values for $\{\alpha\}$ which yields an initial set of pressures $\left(\frac{\Delta p}{q}\right)_1$ shown by point A, Figure 2.1	(1) $\{\alpha\}_o = \{\bar{\alpha}_g\}$ $\left\{\frac{\Delta p}{q}\right\}_1 = \left[\left\lfloor \frac{Q_o}{\bar{\alpha}_g} \right\rceil + \left\lfloor Q_1 \right\rceil + \left\lfloor \frac{Q_n}{\bar{\alpha}_g} \right\rceil \right] \{\bar{\alpha}_g\}$ (2.10)
(2) Use initial pressures to obtain a a set of initial loads $\{P_Z\}_1$ and determine the first set of structural influence coefficients $\left[\delta_{\alpha Z}\right]_1$. This computation is an iteration process in itself the results of which are shown on Figure 2.1 by the straight line labeled BE.	(2) $\{P_Z\}_1 = q \left\lfloor R \right\rceil \left\{\frac{\Delta p}{q}\right\}_1$ (2.4) $\left[\delta_{\alpha Z}\right]_1 = \left[\delta_{\alpha Z}(P_{Z_1})\right]$
(3) Using $\{\alpha\}_o$ and $\left[\delta_{\alpha Z}\right]_1$ compute $\left[\Gamma\right]_1$	(3) $\left[\Gamma\right]_1 = \left[\delta_{\alpha Z}\right]_1 \left\lfloor R \right\rceil \left[\left\lfloor \frac{Q_o}{\bar{\alpha}_g} \right\rceil + \left\lfloor Q_1 \right\rceil + \left\lfloor \frac{Q_n}{\bar{\alpha}_g} \right\rceil \right]$ (2.18)

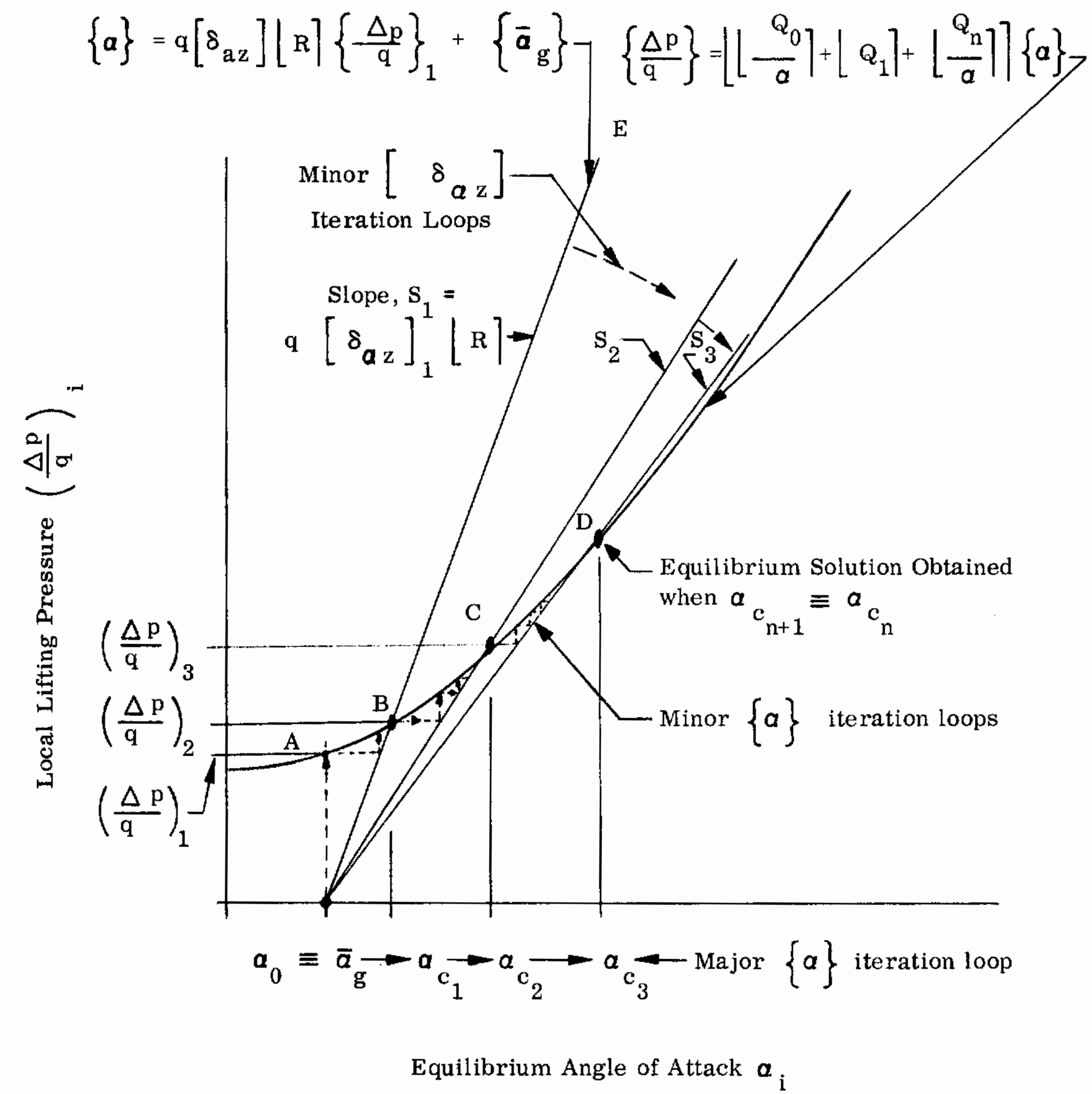

Figure 2.1. Illustration of Iteration Technique

Steps	Equation
(4) Using $\{\alpha\}_o$ and $[\Gamma]_1$ compute $\{\alpha\}_1$ using Equation (2.22).	(4) $\{\alpha\}_1 = \left[\left\lfloor 1 \right\rceil + q[\Gamma]_1\right]\{\bar{\alpha}_g\} + q^2[\Gamma]_1^2\{\bar{\alpha}_g\}$ (2.22)
(5) Repeat steps 3) and 4) using $\{\alpha\}_1$ in place of $\{\alpha\}_o$. Continue process until $\{\alpha\}$ converges to a set, $\{\alpha_{c_1}\}$, as shown by the dashed line path from point A to B.	(5) $[\Gamma]_2 = [\delta_{\alpha Z}]_1 \left\lfloor R \right\rceil \left[\left\lfloor \frac{Q_o}{\alpha_1} \right\rceil + \left\lfloor Q_1 \right\rceil + \left\lfloor \frac{Q_n}{\alpha_1} \right\rceil\right]$ (2.18) $\{\alpha\}_2 = \left[\left\lfloor 1 \right\rceil + q[\Gamma]_2\right]\{\alpha\}_1 + q^2[\Gamma]_2^2\{\alpha\}_1$ (2.22)

etc.

(6) Using $\{\alpha_{c_1}\}$ as a new set of initial values repeat steps (1) to (5) resulting in the the path B to C yielding $\{\alpha_{c_2}\}$.

(7) Compare $\{\alpha_{c_2}\}$ with $\{\alpha_{c_1}\}$ in accordance with some convergence criteria.

(8) Repeat steps (6) and (7) until $\{\alpha_{c_{n+1}}\} = \{\alpha_{c_n}\}$ as shown by point D.

Several features of the iteration scheme should be pointed out. First, the method of solution contains three iteration loops. The minor structures or $[\delta_{\alpha Z}]$ loop (discussed in Section 2.4) is used to determine sets of structural influence coefficients (which depend on $\{P_Z\}$). Intermediate sets of α's are obtained in the minor $\{\alpha\}$ loop shown by the dashed line paths in Figure 2.1. The major $\{\alpha\}$ loop compares successive values of $\{\alpha_{c_n}\}$ obtained from the minor $\{\alpha\}$ loop in order to define the final set of converged $\{\alpha\}$'s. When structural nonlinearities are neglected only one set of $[\delta_{\alpha Z}]$ are obtained, represented by line BE for example. In this instance the above iteration scheme resembles the nonlinear lifting pressure component method developed in Reference 16.

Although Equation (2.22) was used in the illustrative example, either Equation (2.19), or any of Equations (2.24) can be used. The choice of one solution type over another can only be based on the judgment of the analyst and on the type of analysis being conducted. Consideration of structural nonlinearities greatly increases machine time thus, it is recommended that initial analyses be made using the closed form solution (Equation 2.19), or series type solutions, m = 0 or m = 1. Tables 4.2 and 4.3 list IBM 7090 machine time for the analyses conducted in this study. It is seen that a relatively large amount of machine time is required to effect a solution which includes both nonlinear aerodynamic and structural behavior.

The iteration procedure illustrated above will usually converge, for a diverging type surface, for values of dynamic pressure less than the nonlinear divergence dynamic pressure q_{D_n}. This is not a shortcoming of the method since any mathematical solution for $q \geq q_{D_n}$ does not represent a physical condition. In other words, mathematical divergence of the iteration procedure is coincident with physical divergence. In the case of a nondiverging type surface, however, it is possible for the iteration procedure not to converge for certain values of q even though a physical equilibrium situation exists for these values of q. In such cases it may be necessary to use Equation (2.19) as the basic iteration equation, or in more extreme cases when even iteration of Equation (2.19) does not converge, recourse to some alternate iteration technique may be required. Additional discussions of these convergence problems are given in References 12 and 16.

2.4 STRUCTURAL ANALYSIS PROCEDURE

2.4.1 Scope

The basic objective of the structural analysis portion of the complete aeroelastic analysis procedure is to accept, as input, the loadings $\left\{ P_Z \right\}$ at the planform reference points and derive and furnish as output the streamwise slope influence coefficients $\left[\delta_{\alpha Z} \right]$.

In computing the structural response, the following limitations prevail:

(1) The wing may be of irregular planform, of either solid or built-up construction, with nonuniform thickness. If the wing is built-up, the internal members (spars, ribs) may be arbitrarily oriented, but the skins are analytically represented as a single solid plate subjected to bending and mid-

plane stress. Only a half-span of the wing, which may extend to the fuselage centerline, may be treated. A hypothetical wing of this type is illustrated in Figure 2.2.

(2) A restraint against linear or rotational displacement may be specified for any designated planform reference point. This permits analysis of a wing supported at the root butt extending through to the fuselage centerline.

(3) Control surfaces are not explicitly considered, but their effects may be recognized in the form of applied loads at the attachment points.

(4) Temperatures may have an arbitrary variation throughout the wing.

(5) The built-in (initial) displacements of the wing from a non-planar surface can be considered.

(6) The analysis will account for the effects of thermal and large deflection force systems on stiffness.

The analysis does not account for nonlinear material properties, vertical shear displacements, cutouts, or stringer-reinforced skins, although the effects of the latter two conditions can be dealt with in an approximate manner. It is a simple matter to revise the analysis to account for vertical shear deflections but the resulting complexity does not appear justified in view of the insignificance of this phenomena for the class of structures in question.

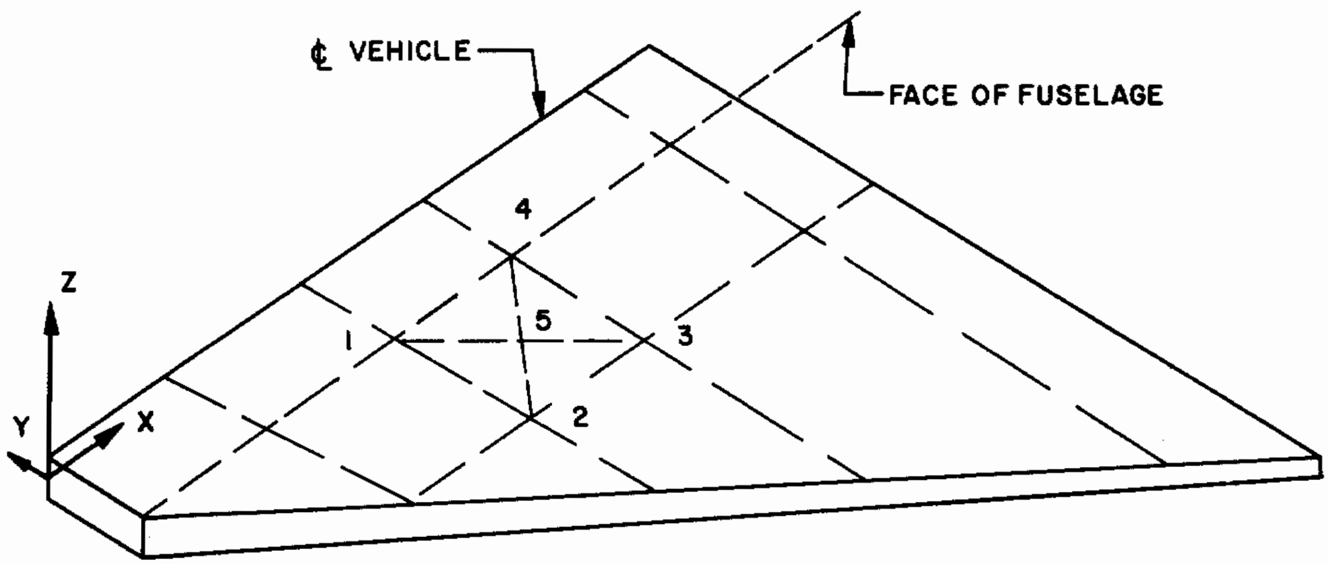

Figure 2.2. Hypothetical Delta Wing

The method of structural analysis employed here is known as the "displacement" or "direct stiffness" approach. Details for linear, unheated analysis have been given in Reference 25; extensions to account for heated, large deflectional behavior were described in Reference 4. The concepts are outlined below.

2.4.2 Basic Concepts

Consider first the analysis of a structure for linear elastic behavior. The structure to be analyzed is represented as an assemblage of simple structural elements. The computer program associated with this study is limited to use of prismatic (beam) members and triangular and rectangular plate elements for idealization purposes. The elements are pictured in Figure 2.3.

It is possible, for each element, to formulate relationships between the displacements of points on the boundary of the element and forces acting at these points. The equations for any type of element can be compactly expressed in the single matrix equation.

$$\left\{ F \right\} = \left[k \right] \left\{ \Delta \right\} \qquad (2.25)$$

where $\left\{ F \right\}$ and $\left\{ \Delta \right\}$ represent the boundary ("node") point forces and displacements, respectively, and $\left[k \right]$ is the "element stiffness matrix."

The elements are assembled to form the complete analytical model of the structure by joining all elements at their respective juncture points, applying in the process the requirements of juncture point equilibrium and compatibility. Thus, the components of internal loads $\left\{ F \right\}$ and external loads $\left\{ P \right\}$ at each point are related by equilibrium requirements, i.e., $\sum F_X = P_X$, etc. The respective coordinate displacements of the corner points of all elements meeting at a point are equal, a requirement that satisfies compatibility. The net effect is that the stiffness matrix, $\left[k \right]$, for the complete structure can be assembled by merely adding element stiffness coefficients having identical subscripts. This results in a set of equations:

$$\left\{ P \right\} = \left[K \right] \left\{ \Delta \right\} \qquad (2.26)$$

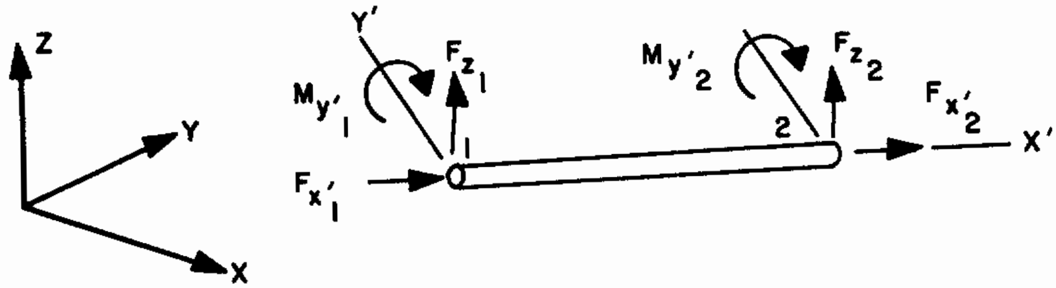

A. AXIAL FORCE AND FLEXURAL ELEMENT

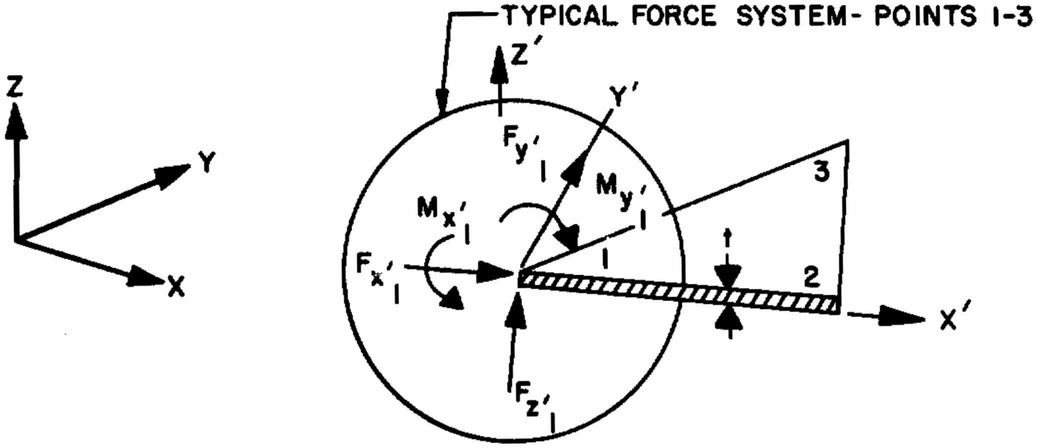

B. TRIANGULAR PLATE ELEMENT

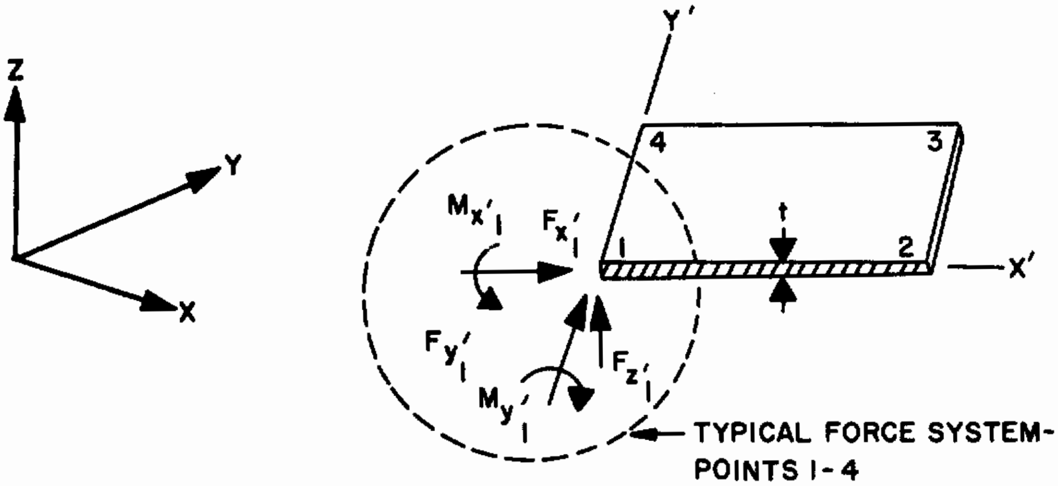

C. RECTANGULAR PLATE ELEMENT

Figure 2.3 Discrete Elements Employed for Analytical Idealization

Force and displacement boundary conditions can be readily imposed by assigning the pertinent P's and Δ's their known values. $[K]$ will be altered in the process, and taking note of this fact without a change in symbolism, the solution to the altered Equation (2.26) becomes:

$$\{\Delta\} = [K]^{-1}\{P\} = [\delta]\{P\} \tag{2.27}$$

where $[\delta]$ represents the set of displacement influence coefficients. The subject approach, as outlined above, possesses certain noteworthy advantages. First, due to the concept of "element stiffness matrices", the computational process is completely automatized--the only required input is the basic physical data of the problem to be solved -- and the boundary conditions do not require the writing of special equations. Secondly, the procedure yields the flexibility coefficients as the direct solution, avoiding the numerous subsequent operations on the direct solution which are required by alternate matrix structural analysis schemes. Furthermore, as will be shown below, the method is fully developed with regard to the structural phenomena of significance to severely heated high-solidity wings.

2.4.3 Concepts for Large-Deflection Heated Wing Analysis

Although the primary concern in the intended analyses relates to displacements normal to the middle surface of the wing, the structural response is importantly affected by behavior in this middle surface. The midplane behavior in question results from nonuniform chordwise and spanwise temperature variations and large deflections. The latter represent, in turn, an influence of the behavior normal to the wing middle surface on deformations in the middle surface. Thus, to account for both midplane and out-of-plane behavior, two analytical models are formed for the same structure:

(1) A model representing deflectional, i.e., "out-of-plane", behavior, and

(2) A model representing midplane behavior.

The use of two elements in place of a single geometric entity merely represents a separation of two classes of deformational behavior. In the model representing deflectional behavior, for example, the triangular plate element (Figure 2.3b) deforms in flexure under node point loads $F_Z{}'$, $M_x{}'$, $M_y{}'$. The node point loads for the model representing midplane behavior are $F_x{}'$ and $F_y{}'$. Corresponding situations apply to the rectangular plate element and to the axial force and flexural elements.

The element relationships for out-of-plane behavior, which have an identical form for each of the three types of elements, are represented by the matrix equation:

$$\begin{Bmatrix} \bar{M}_x{}' \\ \bar{M}_y{}' \\ F_z{}' \end{Bmatrix} = \begin{bmatrix} \left[k_z{}'\right] + \left[n'\right] \end{bmatrix} \begin{Bmatrix} \bar{\alpha}_x{}' \\ \bar{\alpha}_y{}' \\ w' \end{Bmatrix} + \left[k_z{}'\right] \begin{Bmatrix} \bar{\alpha}_{xi}' \\ \bar{\alpha}_{yi}' \\ w'_i \end{Bmatrix} + \begin{Bmatrix} \bar{M}_x{}^{T'} \\ \bar{M}_y{}^{T'} \\ \bar{M}_z{}^{T'} \end{Bmatrix} \qquad (2.28)$$

where $\bar{M}_x{}'$ and $\bar{M}_y{}'$ are moments acting upon the ends of the element. The corresponding angular displacements are $\bar{\alpha}_x{}'$ and $\bar{\alpha}_y{}'$. "Primes" are employed with all moments, forces, and displacements to indicate they are oriented in a coordinate system affixed to the element ("local" coordinates). The "bars" on the M terms indicate these to be quantities associated with the element, i.e., "internal" quantities; the corresponding external moments are unbarred. The vertical forces and displacements are represented by $F_z{}'$ and w'. Sign conventions for the moments, forces and displacements are illustrated in Figure 2.3.

The stiffness of the element for flexure alone is embodied in the matrix $\left[k_z{}'\right]$. The individual elements ($k_{ij}{}'$) of $\left[k_z{}'\right]$ are based only on the material properties and element dimensions. The effect of midplane forces on deflectional stiffness is accounted for by adding an "incremental" stiffness $\left[n'\right]$ to the basic stiffness $\left[k_z{}'\right]$. In simplest terms, the matrix $\left[n'\right]$ represents the out-of-plane components of midplane forces. Hence, the individual elements ($n_{ij}{}'$) of $\left[n'\right]$ are a function of the midplane internal forces (described in a subsequent paragraph) and dimensions of the element.

Built-in (initial) displacements of the wing are listed in the column $\left\{ \alpha'_{xi}, \alpha'_{yi}, w'_i \right\}$. These must be premultiplied by the basic stiffness matrix $\left[k_z{}'\right]$ in representing their role in the force-displacement equations.

Finally, the node point moments and forces required to restrain fully the element against thermal expansion under the permissible temperature profile are listed in the column $\left\{ \bar{M}_x^{T'}, \bar{M}_y^{T'}, F_z^{T'} \right\}$.

Formulations of Equation (2.28) for the beam segment and the triangular and rectangular plate elements are discussed later in the present section and are detailed in Reference 17.

Prior to the assembly of the elements into a master stiffness matrix, the relationships for each element must be transformed from local coordinates into the coordinates of the complete structure (system coordinates). Standard procedures for coordinate transformation, as described in Reference 25 and elsewhere are applied. When transformations have been applied the resulting form of the element equations is identical to that shown in Equation (2.28), less the primes

$$\begin{Bmatrix} \bar{M}_x \\ \bar{M}_y \\ F_z \end{Bmatrix} = \Big[[k_z] + [n] \Big] \begin{Bmatrix} \bar{\alpha}_x \\ \bar{\alpha}_y \\ w \end{Bmatrix} + [k_z] \begin{Bmatrix} \bar{\alpha}_{xi} \\ \bar{\alpha}_{yi} \\ w_i \end{Bmatrix} + \begin{Bmatrix} \bar{M}_x^{T'} \\ \bar{M}_y^{T'} \\ F_z^{T'} \end{Bmatrix} \tag{2.29}$$

Assembly of the element relationships for out-of-plane behavior for the entire structure leads to:

$$\begin{Bmatrix} M_x \\ M_y \\ P_z \end{Bmatrix} = \Big[[K_z] + [N] \Big] \begin{Bmatrix} \alpha_x \\ \alpha_y \\ w \end{Bmatrix} + [K_z] \begin{Bmatrix} \alpha_{xi} \\ \alpha_{yi} \\ w_i \end{Bmatrix} + \begin{Bmatrix} M_x^T \\ M_y^T \\ P_z^T \end{Bmatrix} \tag{2.30}$$

where $\left\{ M_x, M_y, P_z \right\}$ represents applied normal loads and bending moments about axes in the wing plane and $\left\{ M_x^T, M_y^T, P_z^T \right\}$ represents corresponding quantities arising from the temperature gradient through the wing thickness. The displacements $\left\{ \alpha_x, \alpha_y, w \right\}$ are the angular and vertical displacements at the reference points. The objective is to invert $\Big[[K_z] + [N] \Big]$ and to evaluate $\left\{ \alpha_x, \alpha_y, w \right\}$ thusly:

$$\begin{Bmatrix} \alpha_x \\ \alpha_y \\ w \end{Bmatrix} = \left[\left[K_z\right] + \left[N\right] \right]^{-1} \left\{ \begin{Bmatrix} M_x \\ M_y \\ P_z \end{Bmatrix} - \left[K_z\right] \begin{Bmatrix} \alpha_{xi} \\ \alpha_{yi} \\ w_i \end{Bmatrix} - \begin{Bmatrix} M_x^T \\ M_y^T \\ P_z^T \end{Bmatrix} \right\} \tag{2.31}$$

All quantities on the right-hand side of Equation (2.31), with the exception of $\left[N\right]$, are fixed by the geometric, temperature and material property data. The matrix $\left[N\right]$ is dependent on the middle surface internal forces, which, as will be shown below, are in turn dependent upon the angular displacements $\left\{\alpha_x, \ \alpha_y\right\}$ and therefore dependent upon the solution to Equation (2.31). (The angular displacements $\left\{\alpha_y\right\}$ are identical to the angular elastic deformation $\left\{\alpha_s\right\}$, Equation (2.3)). Consequently, the solution process must be conducted in an iterative manner, whereby Equation (2.31) is repeatedly solved for more-improved values of $\left[N\right]$ that evolve from counterpart successive solutions for midplane behavior. The process continues until convergence is achieved. While it would appear that the statement of Equation (2.31) is applicable to any one of the required successive solutions, experience has shown that it will often not lead to a convergent solution. This experience is detailed in Reference 14. An appropriate solution technique, developed in connection with the study of Reference 14, is discussed following a review of the midplane analysis scheme.

The element relationships for midplane behavior, which have an identical form for each of the three types of elements, are represented by the matrix equation

$$\begin{Bmatrix} F_x' \\ F_y' \end{Bmatrix} = \left[k_{xy}'\right] \begin{Bmatrix} u' \\ v' \end{Bmatrix} + \begin{Bmatrix} F_x^{T'} \\ F_y^{T'} \end{Bmatrix} + \begin{Bmatrix} F_x^{\Delta'} \\ F_y^{\Delta'} \end{Bmatrix} + \begin{Bmatrix} F_{xi}^{\Delta'} \\ F_{yi}^{\Delta'} \end{Bmatrix} \tag{2.32}$$

Where F_x' and F_y' are the element end (or corner) point forces and u' and v' are the corresponding displacements. The primes again indicate that the relationships pertain to coordinate directions fixed in one edge of the element. Element stiffness is embodied in the matrix $\left[k_{xy}'\right]$; individual terms of this matrix are a function of the element geometry and the material properties. The thermal forces, $F_x^{T'}$ and $F_y^{T'}$, arise from the element average temperatures. Physically, they represent the forces necessary to provide full restraint of the element against expansion due to the temperature of the element above a reference value of zero. $F_x^{\Delta'}$ and $F_y^{\Delta'}$ are "large deflection" forces and represent the force necessary to maintain the planform dimensions of the middle surface in the presence of a curvature of the middle surface due to out-of-plane behavior. The individual terms of $F_x^{\Delta'}$ and $F_y^{\Delta'}$ are a function of the element angular displacements, $\bar{\alpha}_x'$ and $\bar{\alpha}_y'$, as these are determined in the out-of-plane analysis. F_{xi}^{Δ} and $F_{yi}^{\Delta'}$ are similarly defined, except that the displacements here are the built-in displacements of the wing middle surface. Furthermore, the reference point linear displacements w_i are drawn upon in a machine calculation of the corresponding angular displacements $\bar{\alpha}_{xi}'$ and $\bar{\alpha}_{yi}'$.

Formulations of Equation (2.32) for the axial force member and for the triangular and rectangular plate elements in plane stress are discussed in section 2.45 and are detailed in Reference 17. When the element relationships have been transformed from local to system coordinates the resulting relationships have an appearance identical to Equation (2.32), with the absence of primes.

The completely assembled equations for midplane behavior have the following form:

$$\begin{Bmatrix} P_x \\ P_y \end{Bmatrix} = \begin{bmatrix} K_{xy} \end{bmatrix} \begin{Bmatrix} u \\ v \end{Bmatrix} + \begin{Bmatrix} P_x^T \\ P_y^T \end{Bmatrix} + \begin{Bmatrix} P_x^{\Delta} \\ P_y^{\Delta} \end{Bmatrix} + \begin{Bmatrix} P_{xi}^{\Delta} \\ P_{yi}^{\Delta} \end{Bmatrix} \tag{2.33}$$

where $\left\{ P_x, P_y \right\}$ are applied loads in the midplane, $\left\{ P_x^T, P_y^T \right\}$ are the total thermal loadings, $\left\{ P_x^{\Delta}, P_y^{\Delta} \right\}$ and $\left\{ P_{xi}^{\Delta}, P_{yi}^{\Delta} \right\}$ are the total loadings due to elastic and built-in displacements, and $\left\{ u, v \right\}$ are the midplane displacements of the reference points. The solution to Equation (2.33) can be written as

$$\begin{Bmatrix} u \\ v \end{Bmatrix} = \begin{bmatrix} K_{xy} \end{bmatrix}^{-1} \left\{ \begin{Bmatrix} P_x \\ P_y \end{Bmatrix} - \begin{Bmatrix} P_x^T \\ P_y^T \end{Bmatrix} - \begin{Bmatrix} P_x^{\Delta} \\ P_y^{\Delta} \end{Bmatrix} - \begin{Bmatrix} P_{xi}^{\Delta} \\ P_{yi}^{\Delta} \end{Bmatrix} \right\} \tag{2.34}$$

The midplane displacements are thereby determined. They can then be substituted back into the element relationships (Equation (2.32)) to yield the midplane forces on the element. The latter are a necessary input to the out-of-plane analysis.

2.4.4 Solution Procedure

A solution for the structural response can begin with a knowledge of the rigid wing aerodynamic loads $\left\{ P_z \right\}$. (A more fundamental, alternative beginning would be to determine the slope influence coefficients $\left[\delta \alpha_z \right]$ from a linear analysis and employ these in a first evaluation of flexible wing airloads $\left\{ P_z \right\}$). The geometric and material property data, as well as the reference point temperatures, must also be known.

The structural analysis can commence in either the midplane or out-of-plane portions. Generally, it is efficient to begin with a midplane analysis for the thermal stresses. Thus, a solution to Equation (2.33) is effected with $\left\{ P_x, P_y \right\} = \left\{ P_x^{\Delta}, P_y^{\Delta} \right\} = \left\{ P_{xi}^{\Delta}, P_{yi}^{\Delta} \right\} = 0$, yielding

$$\left\{ u^T, v^T \right\} = -\left[K_{xy} \right]^{-1} \left\{ P_x^T, P_y^T \right\} \tag{2.33a}$$

The inverse $\left[K_{xy} \right]^{-1}$ is of fixed value and is employed in subsequent cycles of the computational process where $\left\{ P_x^{\Delta}, P_y^{\Delta} \right\} \neq 0$. The solution $\left\{ u^T, v^T \right\}$ is employed to define the midplane thermal stresses and these are used in evaluation of an incremental stiffness $\left[N_T \right]$ related only to the thermal stresses. The out-of-plane stiffness equations (Equation 2.30) can therefore be constructed in the form: $(M_x = M_y = 0)$

$$\begin{Bmatrix} 0 \\ 0 \\ P_z \end{Bmatrix} = \left[K_z + N_T \right] \begin{Bmatrix} \alpha_x \\ \alpha_y \\ w \end{Bmatrix} + \left[K_z \right] \begin{Bmatrix} \alpha_{x_i} \\ \alpha_{y_i} \\ w_i \end{Bmatrix} + \begin{Bmatrix} M_x^T \\ M_y^T \\ P_z^T \end{Bmatrix} \tag{2.30a}$$

For which the solution is

$$\begin{Bmatrix} \alpha_x \\ \alpha_y \\ w \end{Bmatrix}_o = \left[K_z + N_T \right]^{-1} \left\{ \begin{Bmatrix} 0 \\ 0 \\ P_z \end{Bmatrix} - \begin{Bmatrix} M_x^T \\ M_y^T \\ P_z^T \end{Bmatrix} - \left[K_z \right] \begin{Bmatrix} \alpha_{x_i} \\ \alpha_{y_i} \\ w_i \end{Bmatrix} \right\} \tag{2.31a}$$

where $\left\{ \alpha_x, \alpha_y, w \right\}_o$ is the initial solution for displacements.

Certain considerations associated with the above solution should be noted. First, the analysis is, as yet, entirely linear. Secondly, the midplane thermal stresses which lead to the evaluation of $\left[N_T \right]$ have, in general, a destabilizing effect. Thus, the combination $\left[K_z + N_T \right]$ may be a singular matrix if the midplane thermal stresses are very severe and the solution approach described above will not work. In such a case the incremental stiffness due to "large deflection" midplane forces has a stabilizing effect and must be introduced into the out-of-plane analysis simultaneously with the midplane thermal stress effect. To do this, one can begin the analysis with the out-of-plane solution (without $\left[N_T \right]$) thereby developing displacements needed for a first guess determination of large-deflection midplane stresses. Many alternatives to this approach present themselves.

If $\left[K_z + N_T \right]$ is not singular, the analysis can proceed from Equation (2.31a) above to the evaluation of $\left\{ P_x^{\Delta}, P_y^{\Delta} \right\}$, using for this purpose $\left\{ \alpha_x, \alpha_y \right\}$. With evaluation of $\left\{ P_{x_i}^{\Delta}, P_{y_i}^{\Delta} \right\}$, one obtains the related midplane displacements $\left\{ u^{\Delta}, v^{\Delta} \right\}$, i.e.

$$\left\{ u^{\Delta}, v^{\Delta} \right\} = - \left[K_{xy} \right]^{-1} \left\{ \left\{ P_x^{\Delta}, P_y^{\Delta} \right\} + \left\{ P_{x_i}^{\Delta}, P_{y_i}^{\Delta} \right\} \right\} \tag{2.33b}$$

After solution for the midplane large deflection stresses, based on $\left\{ u^{\Delta}, v^{\Delta} \right\}$, the incremental stiffness ($\left[N_{\Delta} \right]$) associated with large deflection midplane stress is formed. The governing equations for out-of-plane behavior now become:

$$\begin{Bmatrix} 0 \\ 0 \\ P_z \end{Bmatrix} = \left[K_z + N_T\right] \begin{Bmatrix} \alpha_x \\ \alpha_y \\ w \end{Bmatrix} + \left[N_\Delta\right] \begin{Bmatrix} \alpha_x \\ \alpha_y \\ w \end{Bmatrix} + \left[K_z\right] \begin{Bmatrix} \alpha_{x_i} \\ \alpha_{y_i} \\ w_i \end{Bmatrix} + \begin{Bmatrix} M_x^T \\ M_y^T \\ P_z^T \end{Bmatrix} \tag{2.31b}$$

To effect a complete solution, Equation (2.29b) is rearranged and solved in part to yield

$$\begin{Bmatrix} \alpha_x \\ \alpha_y \\ w \end{Bmatrix} = \left[K_z + N_T\right]^{-1} \left\{ \begin{Bmatrix} 0 \\ 0 \\ P_z \end{Bmatrix} - \left[K_z\right] \begin{Bmatrix} \alpha_{x_i} \\ \alpha_{y_i} \\ w_i \end{Bmatrix} - \begin{Bmatrix} M_x^T \\ M_y^T \\ P_z^T \end{Bmatrix} - \left[N_\Delta\right] \begin{Bmatrix} \alpha_x \\ \alpha_y \\ w \end{Bmatrix} \right\} \tag{2.31c}$$

and with use of the solution given by Equation (2.29a)

$$\begin{Bmatrix} \alpha_x \\ \alpha_y \\ w \end{Bmatrix} = \begin{Bmatrix} \alpha_x \\ \alpha_y \\ w \end{Bmatrix}_o - \left[K_z + N_T\right]^{-1} \left[N_\Delta\right] \begin{Bmatrix} \alpha_x \\ \alpha_y \\ w \end{Bmatrix} \tag{2.31d}$$

The matrix $\left[K_z + N_T\right]^{-1}$ is of fixed value for a given thermal environment while the forces $\left\{0, 0, P_z\right\}$ are of fixed value for a given structural analysis sequence. Thus, the only changes which occur as successive recomputations are made for the midplane and out-of-plane displacements are those which take place in $\left[N_\Delta\right]$ in the out-of-plane formulation and $\left\{P_x^\Delta, P_y^\Delta\right\}$ in the midplane formulation.

It is convenient to regard Equation (2.31d) as pertaining to any of the cycles of computation. On the left hand side the displacements are those sought in the ith cycle and are given the subscript i. On the right side, the displacements to be employed are those already determined in the previous cycle of computation and are therefore assigned the subscript (i-1). Also, the matrix $\left[N_\Delta\right]$ will have been computed using midplane stresses derived on the basis of the (i-1)th displacements and is also given in subscript (i-1). Hence, Equation (2.31d), in the form of a general formula, now reads

$$\begin{Bmatrix} \alpha_x \\ \alpha_y \\ w \end{Bmatrix}_i = \begin{Bmatrix} \alpha_x \\ \alpha_y \\ w \end{Bmatrix}_o - \left[K_z + N_T\right]^{-1} \left[N_\Delta\right]_{(i-1)} \begin{Bmatrix} \alpha_x \\ \alpha_y \\ w \end{Bmatrix}_{i-1} \qquad (2.31e)$$

When, in succeeding cycles of computation, the values of $\left\{\alpha_x, \alpha_y, w\right\}_i$ and $\left\{\alpha_x, \alpha_y, w\right\}$ agree to a specified extent, convergence will have been achieved. Then, in order to obtain the required influence coefficients, the finalized solution to Equation (2.31b) is

$$\begin{Bmatrix} \alpha_x \\ \alpha_y \\ w \end{Bmatrix} = \left[K_z + N_T + N_{\Delta_i}\right]^{-1} \left\{ \begin{Bmatrix} 0 \\ 0 \\ P_z \end{Bmatrix} - \left[K_z\right] \begin{Bmatrix} \alpha_{x_i} \\ \alpha_{y_i} \\ w_i \end{Bmatrix} - \begin{Bmatrix} M_x^T \\ M_y^T \\ P_z^T \end{Bmatrix} \right\} \qquad (2.31f)$$

The portion of the inversion which defines relationships between $\left\{\alpha_y\right\}$ and $\left\{P_z\right\}$ is the required set of influence coefficients.* These coefficients are transmitted to the aeroelastic interaction analysis to be employed in the derivation of an improved set of loads $\left\{P_z\right\}$. The improved loads occasion a redetermination of influence coefficients and all aspects of analysis are repeated until covergence of both loads and displacements are accomplished.

* The required set of influence coefficients are based on secant stiffness rather than the tangent stiffness concept. The former is appropriate to static aeroelastic analyses, since these require the relationship between the total P_z and α_y. For dynamic aeroelastic studies, stiffnesses about an equilibrium condition ("tangent stiffnesses") are required. See Reference 14 page 35 for further discussion.

2.4.5 Element Relationships

Force-displacement relationships for the axial force and flexural element, as required for the subject analyses, are developed in detail in References 14 and 26. Relationships for the triangular and rectangular plate elements, however, have been published only for midplane behavior. Hence, a review of the bases for the derivation of triangular and quadrilateral plate element properties is given in the following. Details are presented in Reference 17.

The development of the force-displacement properties for a plate element, for either inplane or out-of-plane behavior, can be accomplished on the basis of assumed displacement or deformational modes for the element. Detailed procedures for transforming such assumptions into element properties are presented in References 27 and 28.

Consider first the quadrilateral in bending. A lateral deflection pattern in the form of a polynomial will be assumed, the number of terms in the polynomial being equal to the number of corner forces acting upon the element. Here (see Figure 2.3) there are three "forces" (F_z', M_x', M_y') at each corner point, or a total of twelve forces. Thus, the 12-term polynomial is chosen as

$$w = f_1 x^3 + f_2 x^2 + f_3 x + f_4 y^3 + f_5 y^2 + f_6 y + f_7 x^3 y + f_8 x^2 y + f_9 xy + f_{10} y^3 x + f_{11} y^2 x + f_{12} \tag{2.35}$$

This function satisfies the differential equation of equilibrium ($\nabla^4 w = \frac{q}{D} = 0$) over the surface of the element. Both the $\left[K_z \right]$ and $\left[n \right]$ matrix follow from the application of the principles of References 27 and 28 to this function. The thermal force column ($\left\{ M_x^T, M_y^T, F_z^T \right\}$) is derived simply through the assumption of a constant thermal moment and by transformation of the distributed edge moments into node point moments.

Development of flexural relationships for the triangle proceeds along the same path as the rectangle. In this case nine forces are involved so that the assumed displacement function is

$$w = a_1 + a_2 x + a_3 y^2 + a_4 y + a_5 x^2 + a_6 x^3 + a_7 y^3 + a_8 xy + a_9 xy^2 \tag{2.36}$$

This function also satisfies the differential equation of equilibrium over the surface of the element. Again, thermal forces and moments are derived on the basis of a constant thermal moment throughout the element.

In the case of midplane behavior the assumptions utilized for the development of the relationships for both elements are those advanced by Turner, et al, in Reference 25. These are assumptions on stress and take the following forms:

For the rectangle

$$\begin{aligned} \sigma_x &= a_1 + a_2 y \\ \sigma_y &= a_3 + a_4 x \\ \tau_{xy} &= a_5 \end{aligned} \tag{2.37}$$

For the triangle

$$\sigma_x = a_1, \quad \sigma_y = a_2, \quad \tau_{xy} = a_3 \tag{2.38}$$

The above stress assumptions are easily transformed into the corresponding assumed displacements by use of Hooke's Law and by integration of the strain-displacement equations. The thermal forces ($\left\{ F_x^{\alpha}, F_y^{\alpha} \right\}$) and large-deflection forces ($\left\{ F_x^{\Delta}, F_y^{\Delta} \right\}$) are derived by assumptions of constant thermal and large-deflection strains, respectively, and by computation of the corner forces as the static equivalents of the corresponding edge stresses.

2.5 DETERMINATION OF DIVERGENCE DYNAMIC PRESSURE AND STABILITY AND CONTROL DERIVATIVES

2.5.1 Divergence Dynamic Pressure

The nonlinear divergence dynamic pressure, q_{D_n}, can be established by use of an approximate procedure. The criterion for divergence was established in Reference 16 as

$$\left\{\frac{\partial \alpha}{\partial q}\right\} = \{\infty\} \tag{2.39}$$

Application of this criterion to Equation (2.15) yields

$$\left\{\frac{\partial \alpha}{\partial q}\right\} = \left[\lfloor 1 \rceil - q\left[\delta_{\alpha z}\right]\lfloor R \rceil\left[\lfloor Q_1 \rceil + \left\lfloor \frac{\partial Q_n}{\partial \alpha} \right\rceil\right]\right]^{-1} \left[\delta_{\alpha z}\right]\lfloor R \rceil\left\{\lfloor Q_o \rceil \{1\} + \lfloor Q_1 \rceil \{\alpha\} + \lfloor Q_n \rceil \{1\}\right\} \tag{2.40}$$

where by examination,the right hand side becomes infinite if either the equilibrium angles of attack or the nonlinear pressure components $\lfloor Q_n \rceil$ become infinite or if the determinant of the inverse matrix vanishes. The value of q which satisfies the latter condition is q_{D_n} which by definition is the reciprocal of the largest eigenvalue of the matrix

$$\left[\left[\delta_{\alpha z}\right]\lfloor R \rceil\left[\lfloor Q_1 \rceil + \left\lfloor \frac{\partial Q_n}{\partial \alpha} \right\rceil\right]\right] \tag{2.41}$$

For linear aerodynamic and structural response this matrix is easily iterated for the divergence dynamic pressure q_{D_ℓ}. Consideration of aerodynamic nonlinearities complicates the iteration process as discussed in Reference 16. Inclusion of both aerodynamic and structural nonlinearities demands an iteration technique which accounts for the variation of $\left[\delta_{\alpha z}\right]$ with $\{P_z\}$ thus increasing the complexity of the technique. The studies of Reference 16 demonstrated the difficulties in obtaining an exact value of q_{D_n} for only aerodynamic nonlinearities. Thus an alternate approach for determining q_{D_n} for the total nonlinear case is in order.

Examination of Equation (2.41) shows that q_{D_n} is a function of the same parameters as the equilibrium angle of attack. The iteration technique described in Section 2.3 will mathematically diverge for values of the different parameters, including q, when the lifting surface experiences physical divergence. Thus, if all parameters are held constant and solutions obtained for the equilibrium angle of attack for increasing values of q, then these solutions will converge for $q < q_{D_n}$. Hence it would seem possible to obtain q_{D_n} as accurately as desired by using smaller increments for q as q_{D_n} is approached. Theoretically this is correct but in practice it was shown that equilibrium solutions for $\{ \alpha \}$ diverge for q somewhat below q_{D_n}. Just where this occurs is dependent on the number of significant figures used in the iteration cycles. (See Reference 16). In any case, however, such a procedure does establish a lower bound for q_{D_n} and this type of solution often provides sufficient information for the analyst.

Another approach, more practical in a sense, is the use of the flexible to rigid lift coefficient ratio of the surface under study. This ratio is a function of the equilibrium angle of attack and is a good indicator of divergence. For given values of q and $\bar{\alpha}_g$, solutions for this ratio may be obtained for the following cases:

(1) Linear aerodynamic and structural response. In this case q_{D_ℓ} can be exactly determined.

(2) Nonlinear aerodynamic and linear structural response.

(3) Linear aerodynamic and nonlinear structural response.

(4) Nonlinear aerodynamic and nonlinear structural response.

It should be recognized of course that when the lift coefficient ratio is less than one, the lifting surface is exhibiting nondiverging type characteristics and is considered not to have a real divergence dynamic pressure. For most practical configurations the trend towards divergence should be obvious from the results obtained from all or some of the four cases listed above. These results will give a good indication of the bounds between which q_{D_n} lies. Quite often q_{D_ℓ} will be an upper bound to q_{D_n}; however, no general conclusion as this can be made since large variations in aerodynamic and structural parameters could result in exceptions to any such general conclusion

Finally, it must be emphasized that the divergence dynamic pressure denotes a condition of neutral stability and as such is a flight condition which a vehicle must not even approach closely. At the divergence condition, the increase in the aerodynamic moment due to an arbitrary change in α_g is balanced by a corresponding increase in the elastic restoring moment. The former is a function of dynamic pressure; the latter is invarient with this parameter. Thus, as a vehicle's speed approaches q_{D_n} the incremental aerodynamic and elastic restoring moments become equal. At speeds above q_{D_n}, the aerodynamic moment increases drastically producing an unstable condition. (See Reference 16 for further discussion.) Hence precise values of q_{D_n} need not be defined. Lower bounds to q_{D_n}, established by the above approaches, should be sufficient to establish flight spectrum boundaries for a vehicle.

2.5.2 Stability and Control Derivatives

The effects of flexibility on static stability and control derivatives under a linear aeroelastic system were presented in detail in Reference 22. Methods for determining these effects with a nonlinear aerodynamic response are given in Reference 16. The following discusses a method for determining these effects for the case of nonlinear aerodynamic and nonlinear structural response.

The derivatives, for the case under consideration, are obtained in the same manner as was described in the above references. That is, for a given set of rigid input angles (See Equation (2.2)), the nondimensional lifting pressures are obtained by using the iteration procedure of Section 2.3. These distributions are integrated to give nondiminsional span loadings, which in turn are integrated to yield either lift or moment coefficients; finally these coefficients are differentiated with respect to the variables of interest to give expressions for the desired stability and control derivatives. Mathematical expressions for the flexible to rigid ratio of C_{L_α} C_{ℓ_δ} and C_{ℓ_β}, for example, for the total nonlinear case under consideration here, are identical to those expressions given in Reference 16, thus, only a brief discussion is needed to indicate how nonlinearities are accounted for. The parameters C_L and C_{L_α} will be used for this discussion.

Following the derivation in Reference 16, the lift coefficient for the main lifting surface (wing) of a flight vehicle due only to angle of attack α_g is given by

$$C_L = \lfloor \bar{I} \rfloor \left\{ \frac{\Delta p}{q} \right\}, \quad \lfloor \bar{I} \rfloor = \lfloor I \rfloor \left\lfloor \frac{c}{\bar{c}} \right\rceil \left\lceil I \right\rceil \tag{2.42}$$

$\lfloor I \rfloor$ and $\lceil I \rceil$ are integrating matrices, $\left\lfloor \frac{c}{\bar{c}} \right\rceil$ is a matrix of wing chords non-dimensionalized by wing average chord. Substitution of Equation (2.10) into Equation (2.42) yields the flexible lift coefficient.

$$C_{L_F} = \lfloor \bar{I} \rfloor \left[\left\lfloor \frac{Q_o}{\alpha} \right\rceil + \lfloor Q_1 \rceil + \left\lfloor \frac{Q_n}{\alpha} \right\rceil \right] \{\alpha\}^* \tag{2.43}$$

Setting $\alpha = \alpha_g$ yields the rigid lift coefficient

$$C_{L_R} = \lfloor \bar{I} \rfloor \left[\left\lfloor \frac{Q_o}{\alpha_g} \right\rceil + \lfloor Q_1 \rceil + \left\lfloor \frac{Q_n}{\alpha_g} \right\rceil \right] \{\alpha_g\}^* \tag{2.44}$$

By definition $C_{L_\alpha} = \dfrac{\partial C_L}{\partial \alpha_{Ref}}$, hence the nonlinear flexible to rigid ratio of lift curve slopes is, for $\lfloor Q_n \rceil = \lfloor Q_2 \rceil \lfloor \alpha^2 \rceil$

$$\left(\frac{C_{L_{\alpha_F}}}{C_{L_{\alpha_R}}} \right)_n = \frac{\lfloor \bar{I} \rfloor \left[\lfloor Q_1 \rceil + 2 \lfloor Q_2 \rceil \right] \left\{ \frac{\partial \alpha}{\partial \alpha_{Ref}} \right\}}{\lfloor \bar{I} \rfloor \left[\lfloor Q_1 \rceil + 2 \lfloor Q_2 \rceil \lfloor \alpha_g \rceil \right] \{1\}} \tag{2.45}$$

since $\left\{ \dfrac{\partial \alpha_g}{\partial \alpha_{Ref}} \right\} = \{1\}$.

* It is noted that for the total nonlinear case, the lifting pressures and lift coefficient are a function of other angles than α_g; e.g., control surface deflection. However in the present development only α_g is being considered, hence it is possible to consider the lift on only one semi-span of the wing to obtain C_{L_α} , otherwise the lift on both semispans would have to be considered. Reference 16 discusses more general cases where coupling between angles is accounted for.

Methods for obtaining the equilibrium angle of attack have been presented in Section 2.3, thus C_{L_F} can be easily determined. However $\left\{ \partial \alpha / \partial \alpha_{Ref} \right\}$ generally cannot be explicity determined and must be obtained by either graphically or numerically differentiating $\{\alpha\}$ with respect to α_{Ref} for each reference point. However $C_{L_{\alpha_F}}$ and $C_{L_{\alpha_R}}$ may be obtained with less labor by applying these differentiating techniques to C_{L_F} and C_{L_R}. These same techniques would be used to obtain C_{ℓ_δ} and C_{ℓ_β} except that the rolling moment coefficient C_ℓ is differentiated with respect to δ or β.

Examination of the above equations shows that the flexible and rigid lift curve slopes are a function of α_g which is a function of α_{Ref}. These quantities are also a function of Mach number and altitude through the dynamic pressure. Non-linear structural response is implicity accounted for in the determination of $\{\alpha\}$ as discussed in Section 2.3. Nonlinear aerodynamic response is explicitly accounted for through Equation (2.10). Thus in practice the effect of these nonlinearities on the stability and control derivatives can be determined by computing $\{\alpha\}$ distributions using the procedure in Section 2.3. and then following the differentiation technique discussed above.

SECTION 3.0

SIMULATION OF NONLINEAR STATIC AEROELASTIC BEHAVIOR

3.1 GENERAL

The most apparent and straightforward approach to experimental determination of the desired aeroelastic data is through testing a flexible wing model in a hypersonic wind tunnel. This approach is not presently feasible nor practical due to the following principle reasons:

(1) Prohibitive cost involved in both model fabrication and wind tunnel operations.
(2) State-of-the-art regarding the fabrication of flexible wind tunnel models for high temperature operation is in its infancy.
(3) The need to develop expensive instrumentation and associated cooling systems to measure static aeroelastic parameters.
(4) The increased number of "wind tunnel runs" required for aeroelastic models.
(5) Reliable hypersonic wind tunnel facilities of relatively large size and long duration times are limited in number, thus a priority for lengthy test times is difficult to obtain. In addition scheduling and lead times become lengthy.
(6) Simulation of all pertinent phenomena cannot be achieved.

Examination of the alternatives to wind tunnel testing led to the development of the system described in this report. This system employs structural test laboratory facilities of the type possessed by major airframe companies and research organizations. It is relatively inexpensive and suitable for wing proportions ranging from model to full scale. The system fulfills two basic criteria. First, it is consistent with the "field" approach wherein the behavior of a lifting surface is represented by designated planform "reference" points. Secondly, it is based on the accepted premise that the hypersonic aerodynamic load at a point is a function of the angle of attack at only that point. It is felt however, that the system described herein could be adapted to simulate other aerodynamic loading conditions such as those that exist in the supersonic flight regime (See References 10 and 11). The technique for simulation of this interaction and the related apparatus and instrumentation facilities are next described. Then a discussion is given of tests actually performed on two thin plate wing models and test data are presented.

3.2 DESCRIPTION OF SIMULATION TECHNIQUE AND RELATED FACILITIES

3.2.1 Test Procedure

Figure 3.1 illustrates a representative lifting surface under test. Numerous reference points have been defined on the wing surface, but attention is directed toward instrumentation concentrated at a typical point, i. This same instrumentation would be located at all the reference points in an actual test setup. Figure 3.2 details the devices, instrumentation, and circuitry associated with the application of load and measurement of angular displacement at point i.

As previously mentioned, the simulation technique described here pertains only to conditions where the aerodynamic load versus angular displacement relationship at each point is independent of such behavior elsewhere. We choose, as a representative applied load versus angular displacement relationship, Equation (2.14) with $Q_n = \overline{Q}_2 \ \alpha^2$. Thus, for point i

$$\left(P_Z\right)_i = \left(P_{Z_o}\right)_i + \left(\overline{Q}_1\right)_i \ \alpha_i + \left(\overline{Q}_2\right)_i \ \alpha_i^2 \qquad (2.14a)$$

Prior to test, the circuitry at each point (Figure 3.2) is provided with settings for $\left(P_{Z_o}\right)_i$, $\left(\overline{Q}_1\right)_i$ and $\left(\overline{Q}_2\right)_i$. These settings are selected, using convenient analysis procedures, to represent aerodynamic conditions at a certain time in a flight profile. Since $\left(P_{Z_o}\right)_i$ produces the effect of a geometric angle of attack (see the discussion preceding Equation (2.16)), the specimen may remain horizontal during test while angle-of-attack variations are introducted by proper adjustment of $\left(P_{Z_o}\right)_i$.

A test begins with the imposition of the system of initial loadings $\left\{P_{Z_o}\right\}$ which immediately cause angular displacements at all points. The magnitude of the initial angular displacement at point i, for example

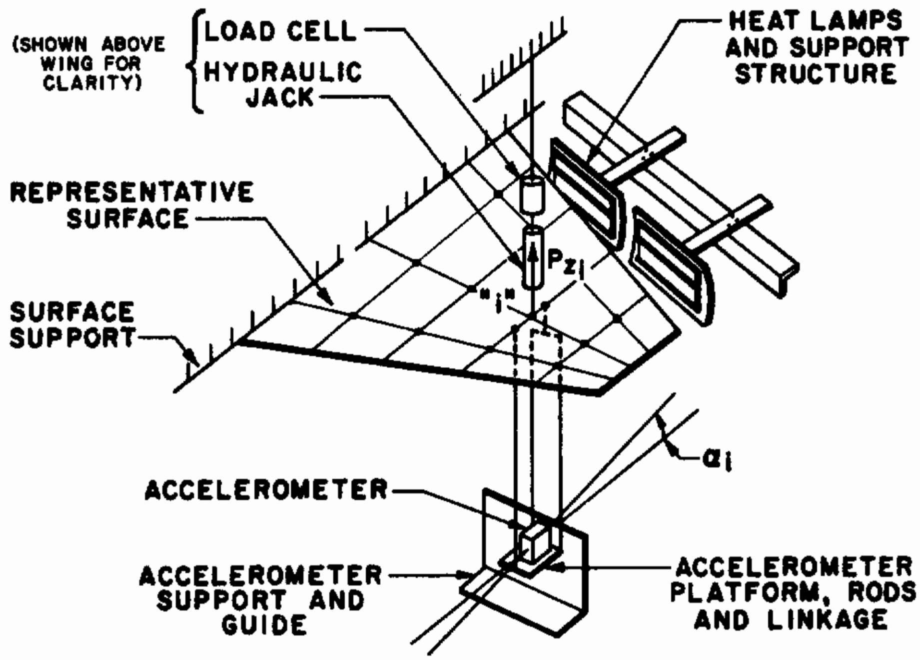

Figure 3.1. Lifting Surface Under Test

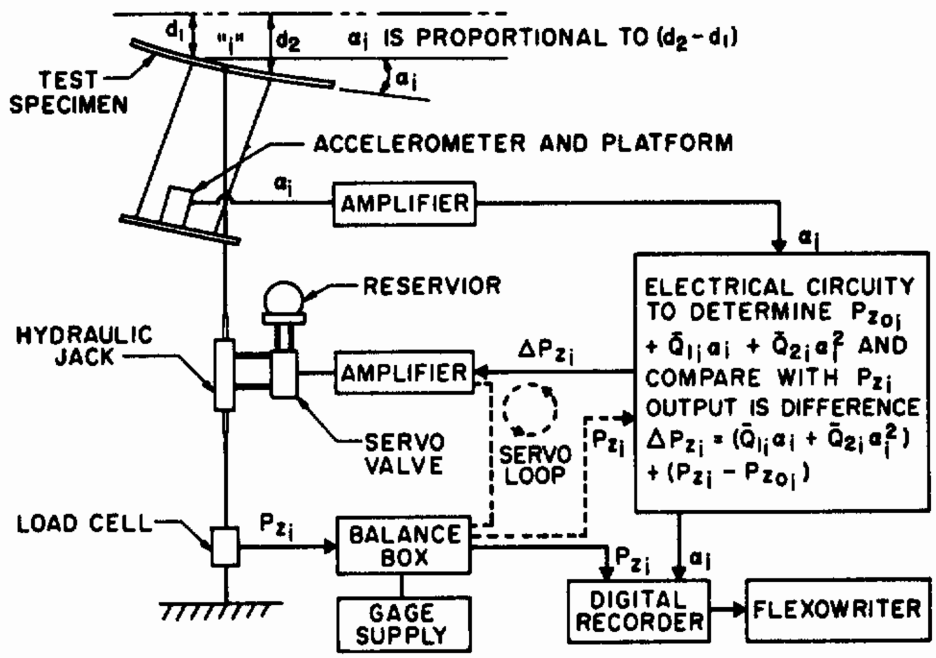

Figure 3.2. Aeroelastic Interaction Test Equipment and Instrumentation

is sensed by an accelerometer arrangement specially designed for this purpose and is transformed into a signal proportional to this magnitude. This signal, in turn, produces a signal for a new load P_{Z_1} and compares this load with the initial load $P_{Z_{o_i}}$. The resulting signal, proportional to ΔP_{Z_i}, actuates a servo control valve and accordingly modifies the loading $P_{Z_{o_i}}$. Thus, a first change in the load is produced as shown in Figure 3.2 and this change $\left(\Delta P_{Z_i}\right)$ is, from Equation (2.14a)

$$\Delta P_{Z_i} = \left(\overline{Q}_1\right)_i \alpha_i + \left(\overline{Q}_2\right)_i \alpha_i^2 \tag{3.1}$$

The load change ΔP_{Z_i} causes additional angular displacement at the reference points. Hence, further adjustments of the load are obtained and the process continues until the surface reaches an equilibrium position. A test cycle concludes with the measurement of equilibrium loads and slopes (i.e., angular displacements).

The simulation of nonlinear aerodynamic behavior is evident in the foregoing procedure. The presence of structural nonlinear behavior is not evident, however. As already emphasized, the significance of structural nonlinearity is dictated by geometric and material properties and other factors influencing stiffness. Under hypersonic flight conditions, a particularly important influence on stiffness results from aerodynamic heating. It is therefore necessary to incorporate aerodynamic heating effects in the subject technique.

Figure 3.1 illustrates the presence of apparatus for the simulation of such effects. The indicated devices are capable of producing in the test specimen an equilibrated temperature distribution of the type that would result, at some instant in a flight plan, from aerodynamic heating. The concept of a "static" (equilibrated) structural temperature distribution is consistent with the concept of static aeroelasticity as a field of investigation concerned with time-independent phenomena. All devices associated with the application and measurement of load and the measurement of slope are located beneath the wing specimen. (For purposes of clarity however, these have been shown above the wing in Figure 3.1). Thus, the areas above and around the specimen are available for the disposition of heating equipment. This arrangement - heating from one side and along the edges - is satisfactory for present purposes since the lifting surfaces in question are "thin", as required for large deflectional behavior, and there is a relatively small difference in temperature between the two wing surfaces due to heat transfer to just one surface.

The major elements of the above simulation scheme are the angular displacement measuring devices (accelerometers), the heating apparatus, the load application devices, and the data measurement equipment.

3.2.2 Angular Displacement Measurement System

A basic instrumentation requirement for this technique is a device which will accurately measure the chordwise angular displacement at a point on the surface of a wing in the presence of elevated temperatures. This requirement was met through the development of the arrangement shown in Figure 3.3 where the accelerometer is the critical element in this system which senses the direction of the gravity vector. The positioning of the accelerometer's sensitive axis in a horizontal direction produces a response in consequence of the acceleration due to gravity when the accelerometer undergoes an angular displacement. This measured acceleration varies as the sine of the angle of displacement and has a maximum value of 1.0 (times g) when the sensitive axis is vertical. For the circumstances of interest, the angular displacements are quite small ($< 5^\circ$) and the accelerometer reading is proportional to the slope itself.

The measurements would be more accurate if the accelerometer were attached directly to the specimen at the point in question, but since elevated temperature tests were to be conducted and the devices would not function properly in the resulting intense heat field, it was decided to mount each accelerometer at a distance from the wing surface. From Figure 3.3, it is seen that the accelerometer is mounted on a 3-1/2 by 5 inch platform, which in turn is attached to the

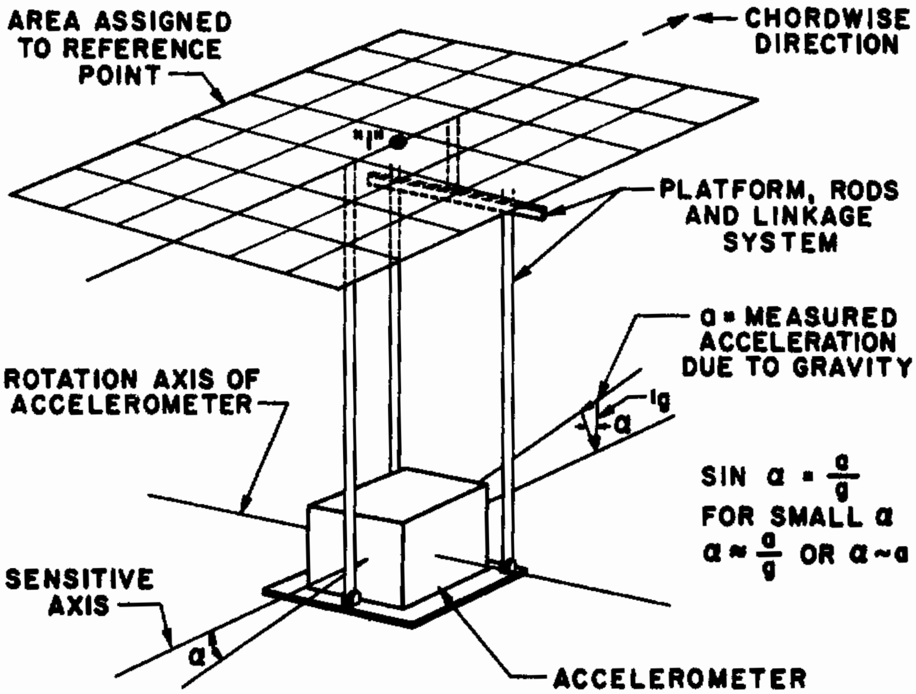

Figure 3.3. Angle Measuring Device

wing surface by means of three rods and a linkage system. The chordwise attachment to the wing surface occurs at two points that are 1-1/2 inches to either side of the associated reference point. The freedom of the platform to move was restricted to a vertical plane and rotation about a spanwise axis. From this arrangement, the accelerometer signal is proportional to $(d_2 - d_1)$, the difference in deflections at the two rod-wing specimen attachment points, rather than at the point i itself.

Measurements taken for the purpose of establishing the accuracy of the above scheme verified that it produces errors of less than 1 percent for angular displacements of up to 5 degrees. Alternative schemes, involving the use of variable permeance extensometers of the type described in Reference 23, were tried and found to yield measurements of insufficient accuracy. Furthermore, those on hand would "bottom-out" under displacements much smaller than those anticipated for actual testing.

3.2.3 Heating Apparatus

A conventional arrangement of radiant heat lamp equipment, identical in most respects to the system described in Reference 23, provided the heating rates which imposed and maintained the temperature distribution in the wing specimen. The basic heating elements were quartz lamps (type T-3) grouped in fixtures around the periphery of the wing specimen as illustrated in Figure 3.1. The desired temperature distribution was established by disposition of the fixtures and reflector plates and by variation of voltage supplied to the various groups of lamps. Four Variac Auto-Transformers, each permitting a range of 0 to 230 volts, proved sufficient for the purposes of voltage regulation.

It should be emphasized that the primary function of the available voltage regulation was to control the stabilized temperature distribution i.e., once a temperature distribution had been established and stabilized, the voltage capabilities were used only to compensate for structural temperature changes resulting from laboratory environmental disturbances.

3.2.4 Load Application System

The load application system for the tests conducted is shown in Figures 3.1 and 3.2. Since these tests were restricted to the measurement of symmetric behavior (i.e., symmetric about the midplane), loads were simultaneously applied, through hydraulic jacks, to corresponding points on each semispan. Each corresponding pair of jacks was connected in parallel to insure a symmetric load condition. A type U-1 Baldwin SR-4 load cell, located between the jack and the support frame, sensed the magnitude of the load and transmitted an electrical signal proportional to this magnitude to the P_{Z_i} versus α_i circuitry and to the data readout equipment for subsequent transformation into digital information. (The data readout equipment will be discussed in the next section.) The support frame for the load application system was extremely stiff, being composed of welded structural steel shapes, and was bolted to tie-down slots embedded in the laboratory floor. (See Figure 3.4.)

3.2.5 Data Reduction Equipment and Techniques

Data recording and reduction procedures for an experimental program of this type can be completely automated with use of widely available equipment. Nevertheless, as a matter of interest and for the sake of completeness, the following brief review of the equipment and procedures employed in the subject program is presented.

As noted previously, the basic output of both the slope measuring device and the load cell is an electrical signal proportional to the reference point slope and load, respectively. Values of these signals were recorded using a flexowriter device (a special typewriter manufactured by the Commercial Controls Corporation, Rochester, New York) which punched data in digital form on output sheets, and also (when desirable) onto paper tape in a form suitable for use as inputs to an IBM 7090 computer. The direct digital output permitted a visual survey of the test data during each test, making it possible to verify that the experiment was proceeding satisfactorily.

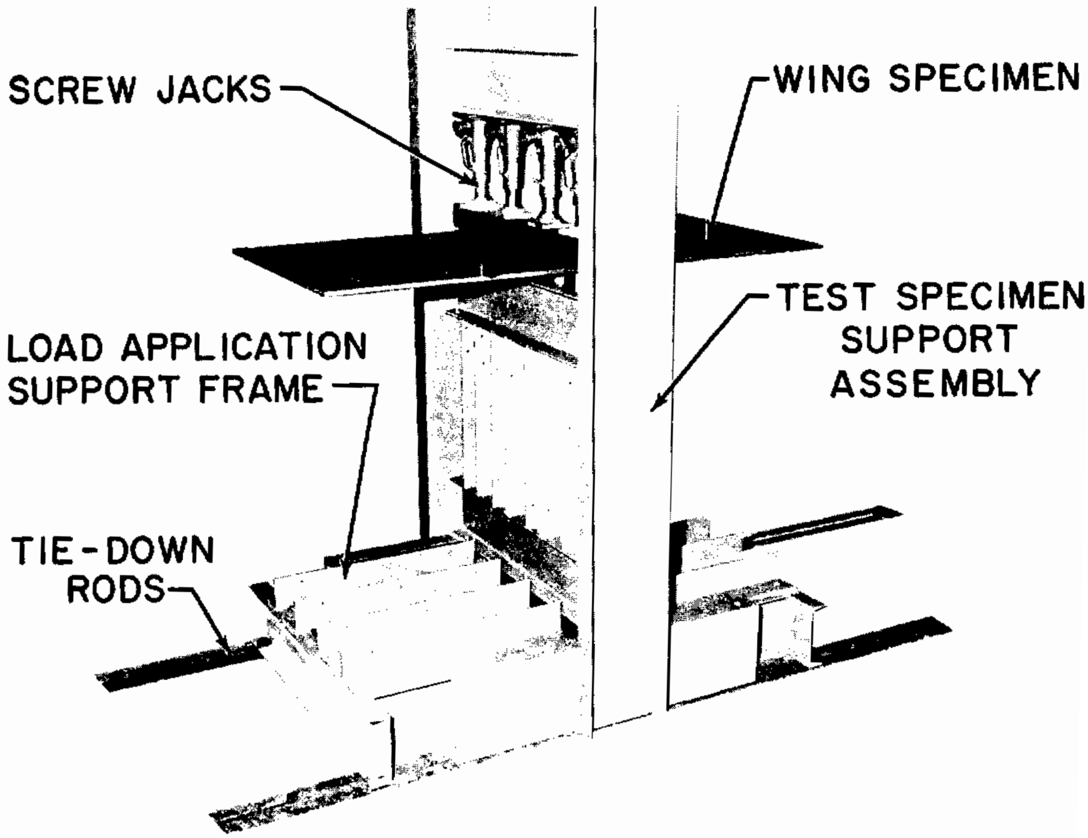

Figure 3.4. Test Specimen Support Structure

The determination of equilibrium loads and angular displacements from the direct digital output of the interaction tests was a simple operation, requiring only the constant of proportionality between the values of the electrical signal produced by the measuring device and the magnitudes of the loads and slopes. In addition to the interaction tests, certain tests were performed with the intent of obtaining displacement (slope) influence coefficients. The punched tape information for these tests was operated upon by the IBM 7090 computer to yield the desired influence coefficients.

3.3 EXPERIMENTAL PROGRAM

The technique described above was employed in an experimental program in which two wing specimens were tested under a variety of room and elevated temperature conditions. The specimens, illustrated in Figure 3.5 are plates of constant thickness; both are of full-span, but for convenience only semispans are shown.

The specimen proportions, material properties, etc., were chosen as a compromise of a number of conflicting requirements, including the need to demonstrate low aspect ratio and large deflection effects while retaining a measure of simplicity for the sake of subsequent test-theory comparisons. Also, it was necessary that the large deflections neither exceed the "travel" limitations and capacity of available instrumentation nor introduce inelastic behavior. After reviewing these factors and the performance of preliminary static aeroelastic and stress analyses, it was decided that one model be of rectangular planform, with an exposed semispan of 30 by 30 inches and 0.538 inch thick, while the second model be of clipped delta planform with semispan of 32 inches, a root chord of 34 inches, and thickness of 0.528 inch. The specimen material is a steel alloy similar in composition to heat treated AISI type 4140 steel.

To provide accurate information for subsequent analytical studies, tests were performed to obtain the material mechanical properties and the coefficient of thermal expansion. Tests were performed at temperatures of 70, 350, 550 and 850°F., on coupons taken from the specimen sheet stock. Interpretation of the

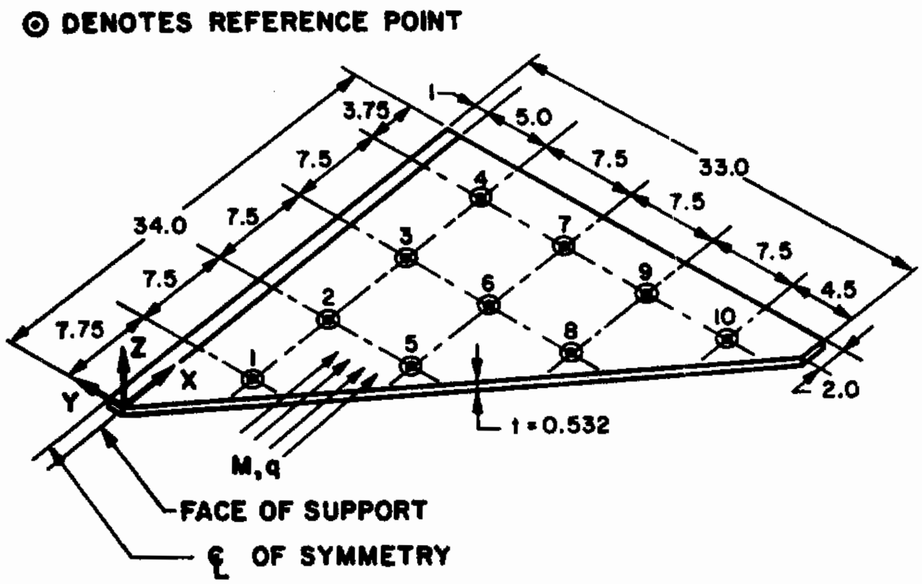

(See Table 3.1 for Assigned Areas)

Figure 3.5b. Delta Wing Planform Specimen

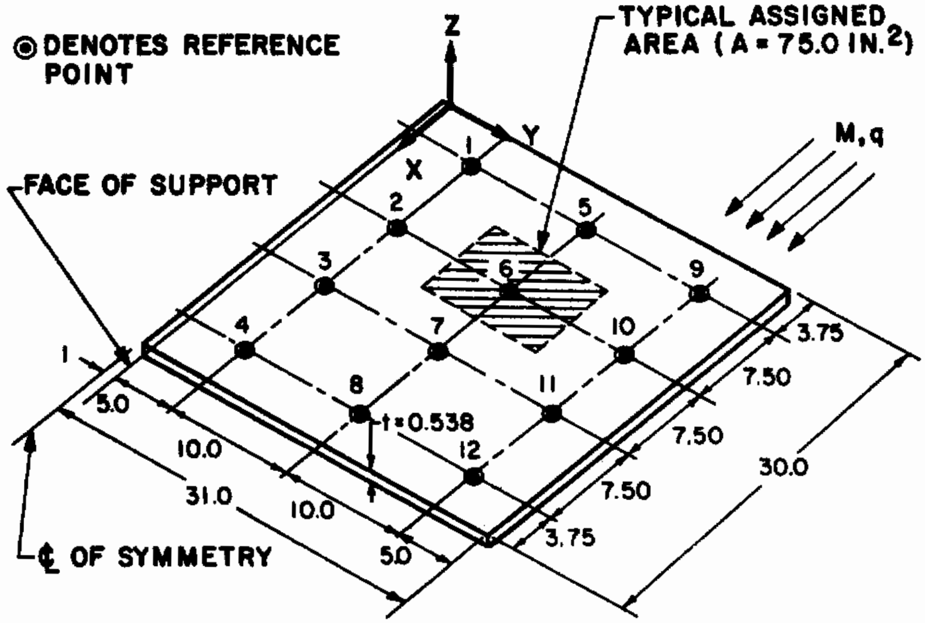

Figure 3.5a. Rectangular Wing Planform Specimen

Figure 3.5. Experimental Program Specimens

resulting data showed that the modulus of elasticity (E,) can be satisfactorily represented as a function of temperature by the expression:

$$E = 30.79 \times 10^{6} - 1.099 \times 10^{4}\, T + 6.693\, T^{2} \tag{3.2}$$

Equation (3.2) is valid in the range of 70 to 800°F.

The average coefficient of thermal expansion was found to be essentially constant through this range of temperatures at a value of 7.0×10^{-6} in./in.°F. The material property tests were used to determine the yield stress and inelastic behavior characteristics of the parent material. This information was compared with the results of stress analyses to assess the possibility of inelastic deformation during test; it was predicted that no significant inelastic deformation would be sustained.

The specimen support assembly, pictured in Figure 3.4, consists of structural shapes which are welded together for rigidity. Screw jacks are used to maintain a clamping pressure on the 2 inch wide specimen support area. This arrangement was designed with the intent of minimizing root flexibility - i.e., to preclude vertical displacement or "roll" rotation of the wing root - while providing a small specimen contact area to minimize heat transfer from the model during elevated temperature tests.

As shown in Figure 3.5, a total of 12 reference points are delineated on the rectangular model semispan and 10 points are employed on the clipped delta semispan. All imposed loading and temperature conditions represented symmetric behavior of the wing as a whole. Thus, the same array of points were delineated on the semispans not shown in Figure 3.5. Each point on the rectangular specimen was assigned a surface area of 75.0 in.^{2}; the areas assigned to points on the clipped delta planform differ from point to point and are listed in Table 3.1.

Tests of the rectangular planform consisted of:

(a) Tests, at room temperature, for slope influence coefficients (care was exercised that the imposed loadings extended only as far as the limits of effectively linear behavior).

TABLE 3.1

DELTA PLANFORM SPECIMEN - ROOM TEMPERATURE TEST PROGRAM
AERODYNAMIC COEFFICIENTS AND RESULTS

Ref. Points	Assigned Area	$\lfloor \bar{Q}_1 \rceil$	$\lfloor \bar{Q}_2 \rceil$	q = 8 psi					
				$\{P_{Z_o}\}_1 = \{449,488,488,505\}$		$\{P_{Z_o}\}_2 = \{573,585,585,606\}$		$\{P_{Z_o}\}_3 = \{649,683,683,733\}$	
				$\{\alpha\}$	$\{P_Z\}$	$\{\alpha\}$	$\{P_Z\}$	$\{\alpha\}$	$\{P_Z\}$
1	62.344	-435	76	-0.2536	568	-0.2975	706	-0.3475	809
2	65.625	-321	80	-0.1368	38	-0.1732	57	-0.2045	68
3	65.625	-275	56	-0.0957	24	-0.1235	32	-0.1411	39
4	65.625	+229	32	+0.0151	2	+0.0126	2	-0.0213	6
5	48.750	-510	24	-0.6500	828	-0.7656	976	-0.9086	1162
6	56.250	-393	48	-0.3514	141	-0.4217	164	-0.5007	208
7	56.250	-432	48	-0.1162	22	-0.1500	55	-0.1900	406
8	48.750	-510	24	-0.7153	858	-0.8434	1020	-1.026	1232
9	56.250	-196	48	-0.4630	89	-0.5644	111	-0.6727	140
10	52.531	-705	62	-0.6425	956	-0.7756	1136	-0.9224	1390
C_{L_F}/C_{L_R}				1.827		1.813		1.873	

Ref. Points	Assigned Area	$\lfloor \bar{Q}_1 \rceil$	$\lfloor \bar{Q}_2 \rceil$	q = 12 psi			
				$\{P_{Z_o}\}_1 = \{100,200,200,200\}$		$\{P_{Z_o}\}_2 = \{150,300,300,300\}$	
				$\{\alpha\}$	$\{P_Z\}$	$\{\alpha\}$	$\{P_Z\}$
1	62.344	-653	114	-0.2083	236	-0.4493	498
2	65.625	-481	120	-0.1285	67	-0.2722	134
3	65.625	-412	84	-0.0828	38	-0.1983	85
4	65.625	+344	48	+0.0126	2	-	-
5	48.750	-766	36	-0.5572	656	-1.1822	1232
6	56.250	-589	72	-0.3182	203	-0.7045	436
7	56.250	-648	72	-0.1381	84	-0.3313	117
8	48.750	-766	36	-0.6325	712	-1.3425	1384
9	56.250	-295	72	-0.3389	112	-0.8609	265
10	52.531	-1058	93	-0.5723	856	-1.2851	1732
C_{L_F}/C_{L_R}				4.237		5.603	

(b) Interaction tests, at room temperature and also in the presence of two elevated temperature environments, for three dynamic pressures over the range of the three aerodynamic coefficients $\left\{ P_{Z_o} \right\}$, $\left\lfloor \bar{Q}_1 \right\rceil$ and $\left\lfloor \bar{Q}_2 \right\rceil$ listed in Table 3.2.

An abbreviated notation is used in Tables 3.1 and 3.2. For example, at room temperature test conditions, Table 3.1, $q = 4$ psi, only the diagonal elements of $\left\lfloor \bar{Q}_1 \right\rceil$, $\left\lfloor \bar{Q}_2 \right\rceil$ are listed. $\left\{ P_{Z_o} \right\}$ is an initial loading column whose nonzero elements at reference points 1, 5, and 9 respectively, are given above the test results $\{\alpha\}$ and $\{P_Z\}$. Thus, a typical

$$\left\{ P_{Z_o} \right\} = \left\{ \begin{array}{c} 450 \\ 0 \\ 0 \\ 0 \\ 300 \\ 0 \\ 0 \\ 0 \\ 375 \\ 0 \\ 0 \\ 0 \end{array} \right\}$$

A total of 27 tests for equilibrium angles of attack and loads are represented. The reasons for the indicated variation in the aerodynamic coefficients and the manner in which they were varied is described below.

Tests of the delta planform conducted during the study covered by this report have been of an exploratory nature and have consisted only of several room temperature tests for a limited range of dynamic pressures and aerodynamic coefficients. These test conditions are listed in Table 3.1.

As indicated in the discussion of the analytical basis of the static aerothermoelastic problem, a reference point angle of attack (α) is a function of the aerodynamic parameters q and α_g, the deformational characteristics of the structure, and the temperature environment. Since it was intended to isolate, insofar as possible, the relative significance of the respective aerodynamic

(Text continued on page 53)

TABLE 3.2

RECTANGULAR PLANFORM SPECIMEN -
TEST PROGRAM AERODYNAMIC COEFFICIENTS AND RESULTS

Test	Reference Points	$\lfloor \bar{Q}_1 \rceil$	$\lfloor \bar{Q}_2 \rceil$	q = 4 psi					
				$\begin{Bmatrix} P_{Z_o} \end{Bmatrix}_1 = \{450,300,375\}$		$\begin{Bmatrix} P_{Z_o} \end{Bmatrix}_2 = \{525,375,450\}$		$\begin{Bmatrix} P_{Z_o} \end{Bmatrix}_3 = \{600,450,525\}$	
				$\{\alpha\}$	$\{P_Z\}$	$\{\alpha\}$	$\{P_Z\}$	$\{\alpha\}$	$\{P_Z\}$
Room Temperature	1	655	46	0.0552	486	0.0427	576	0.0822	656
	2	524	32	0.0637	33	0.0784	41	0.0906	46
	3	262	14	0.0566	15	0.0689	19	0.0812	20
	4	65	7	0.0993	8	0.1140	8	0.1364	10
	5	503	37	0.2362	420	0.2878	524	0.3444	632
	6	346	27	0.2875	99	0.3450	121	0.4075	144
	7	126	14	0.2742	37	0.3334	44	0.3927	52
	8	31	7	0.2814	9	0.3436	11	0.4009	11
	9	288	37	0.4290	504	0.5183	604	0.6121	712
	10	183	27	0.5215	103	0.6090	122	0.7122	144
	11	79	9	0.4258	26	0.5179	31	0.6076	44
	12	26	9	0.3952	10	0.4816	14	0.5752	18
Thermal Test A	1	655	46	0.0402	466	0.0409	544	0.0496	628
	2	524	32	0.0730	36	0.0880	46	0.0975	45
	3	262	14	0.0880	21	0.1108	26	0.1265	32
	4	65	7	0.1482	8	0.1845	11	0.2103	12
	5	503	37	0.2659	433	0.3117	533	0.3710	639
	6	346	27	0.3160	104	0.3911	133	0.4667	161
	7	126	14	0.3778	48	0.4543	60	0.5316	70
	8	31	7	0.3780	11	0.4750	15	0.5575	18
	9	288	37	0.5242	529	0.6220	642	0.7250	752
	10	183	27	0.5645	111	0.6780	138	0.7962	164
	11	79	9	0.5462	48	0.6652	59	0.7799	70
	12	26	9	0.5338	19	0.6388	22	0.7470	27
Thermal Test B	1	655	46	0.0775	501	0.0870	582	0.0938	661
	2	524	32	0.0740	31	0.0904	45	0.1079	46
	3	262	14	0.1008	25	0.1096	27	0.1273	32
	4	65	7	0.1865	12	0.2117	13	0.2774	17
	5	503	37	0.3125	432	0.3547	526	0.3982	626
	6	346	27	0.3692	116	0.4480	148	0.5070	171
	7	126	14	0.4556	60	0.5497	72	0.6300	83
	8	31	7	0.4977	15	0.5897	19	0.6892	23
	9	288	37	0.5999	538	0.7028	646	0.8170	760
	10	183	27	0.6614	129	0.7844	156	0.9149	188
	11	79	9	0.6764	56	0.7982	68	0.9287	80
	12	26	9	0.6501	16	0.7794	22	0.9036	53

TABLE 3.2 (CONT)

Test	q = 6 psi								
				$\{P_{Z_o}\}_1 = \{675,450,563\}$		$\{P_{Z_o}\}_2 = \{188,563,675\}$		$\{P_{Z_o}\}_3 = \{900,675,788\}$	
	Reference Points	$[\bar{Q}_1]$	$[\bar{Q}_2]$	$\{\alpha\}$	$\{P_Z\}$	$\{\alpha\}$	$\{P_Z\}$	$\{\alpha\}$	$\{P_Z\}$
Room Temperature	1	981	69	0.0825	744	0.1125	884	0.1375	1022
	2	785	48	0.1096	82	0.1345	101	0.1594	125
	3	393	21	0.1075	42	0.1325	53	0.1500	62
	4	98	10	0.1900	15	0.2275	18	0.2700	24
	5	754	55	0.4108	760	0.5030	952	0.5876	1140
	6	518	41	0.4700	252	0.5875	324	0.7000	386
	7	188	21	0.4905	82	0.6051	122	0.7171	146
	8	47	10	0.5125	22	0.6325	34	0.7350	40
	9	432	56	0.7093	860	0.8779	1064	1.0565	1268
	10	275	41	0.8610	267	0.9922	313	1.1462	369
	11	118	14	0.7375	91	0.9125	115	1.0625	138
	12	39	14	0.7229	34	0.8885	46	1.0391	58
Thermal Test A	1	981	69	0.0451	707	0.0937	873	0.0960	991
	2	785	48	0.1108	94	0.1533	123	0.1520	124
	3	393	21	0.1575	64	0.2103	80	0.2108	79
	4	98	10	0.2726	28	0.3391	36	0.3511	37
	5	754	55	0.4054	756	0.5690	1218	0.5950	1148
	6	518	41	0.5458	286	0.7400	402	0.7650	411
	7	188	21	0.6437	130	0.8566	179	0.8670	180
	8	47	10	0.7034	39	0.9233	54	0.9357	55
	9	432	55	0.8379	945	1.1200	1213	1.1347	1326
	10	275	41	0.9569	304	1.2624	418	1.2940	428
	11	118	14	0.9479	126	1.2405	174	1.2674	177
	12	39	14	0.9332	46	1.2176	67	1.2375	68
Thermal Test B	1	981	69	0.0775	749	0.1025	890	0.1650	1062
	2	785	48	0.0888	68	0.1100	86	0.1650	133
	3	393	21	0.1594	60	0.1882	72	0.2450	95
	4	98	10	0.3578	35	0.3591	35	0.4350	45
	5	754	55	0.4267	758	0.5522	960	0.7350	1240
	6	518	41	0.5284	272	0.6652	442	0.8550	343
	7	188	21	0.7166	144	0.8371	173	1.0175	222
	8	47	10	0.8298	43	0.9690	52	1.1575	70
	9	432	55	0.8910	950	1.1006	1160	1.4050	1468
	10	275	41	1.0200	317	1.2262	392	1.5180	517
	11	118	14	1.0388	143	1.2275	172	1.5000	219
	12	39	14	1.0630	56	1.2450	68	1.4980	92

TABLE 3.2 (CONT)

q = 8 psi									
Test	Reference Points	$\lfloor \bar{Q}_1 \rfloor$	$\lfloor \bar{Q}_2 \rfloor$	$\{P_{Z_o}\}_1 = \{600,300,450\}$		$\{P_{Z_o}\}_2 = \{750,450,600\}$		$\{P_{Z_o}\}_3 = \{900,600,750\}$	
				$\{\alpha\}$	$\{P_Z\}$	$\{\alpha\}$	$\{P_Z\}$	$\{\alpha\}$	$\{P_Z\}$
Room Temperature	1	1308	91	0.0643	686	0.1031	880	0.1196	1001
	2	1047	64	0.0993	100	0.1415	147	0.1818	192
	3	524	27	0.0991	54	0.1413	75	0.1755	74
	4	131	13	0.1944	24	0.2616	33	0.3146	41
	5	1005	73	0.3458	660	0.4950	968	0.6197	1217
	6	691	55	0.4431	305	0.6194	439	0.7923	577
	7	251	27	0.4800	122	0.6650	177	0.8443	221
	8	63	14	0.4957	34	0.6960	50	0.8763	64
	9	576	73	0.6428	832	0.9132	1192	1.1713	1370
	10	366	55	0.7612	466	1.0448	656	1.2818	561
	11	157	18	0.7165	118	1.0056	172	1.2504	218
	12	52	18	0.7025	46	0.9785	70	1.2246	85
Thermal Test A	1	1308	91	0.0360	636	0.0632	823	0.0967	1010
	2	1047	64	0.0959	100	0.1374	148	0.1887	200
	3	524	27	0.1432	42	0.1987	57	0.2440	72
	4	131	13	0.2492	33	0.3244	45	0.3973	55
	5	1005	73	0.3174	607	0.4881	949	0.6781	1272
	6	691	55	0.4427	305	0.6403	460	0.8313	606
	7	251	27	0.5864	157	0.7931	219	0.9905	277
	8	63	14	0.6544	48	0.8852	68	1.0911	88
	9	576	73	0.7361	880	1.0312	1229	1.3585	1586
	10	366	55	0.8312	342	1.1574	500	1.4627	657
	11	157	18	0.8553	154	1.1658	215	1.4483	274
	12	52	18	0.8662	60	1.1720	88	1.4520	115
Thermal Test B	1	1308	91	0.0520	670	0.0823	856	0.1381	1067
	2	1047	64	0.0735	83	0.1134	118	0.1689	188
	3	524	27	0.1564	41	0.2214	115	0.2879	151
	4	131	13	0.1570	38	0.4213	58	0.5128	69
	5	1005	73	0.3245	604	0.4970	940	0.6930	1317
	6	691	55	0.4687	317	0.6930	486	0.9299	687
	7	251	27	0.6559	177	0.9412	259	1.2000	347
	8	63	14	0.7684	56	1.0980	86	1.3679	115
	9	576	73	0.7472	877	1.1182	1284	1.5041	1744
	10	366	55	0.8993	364	1.3127	565	1.6898	767
	11	157	18	0.9532	170	1.3270	253	1.7231	328
	12	52	18	0.9814	69	1.3981	109	1.7557	148

TABLE 3.2 (CONT)

Notes:

1. Aerodynamic coefficients designated by $\{P_{Z_o}\}$ in pounds, $\lfloor \bar{Q}_1 \rfloor$ in pound/degree $\lfloor \bar{Q}_2 \rfloor$ in pound/(degrees)^2. $\{P_{Z_o}\}$ values are initial loadings at Reference points 1, 5, 9,

$$\text{e.g.,} \left\{ P_{Z_o} \right\} = \begin{Bmatrix} 450 \\ 0 \\ 0 \\ 0 \\ 350 \\ 0 \\ 0 \\ 0 \\ 375 \\ 0 \\ 0 \\ 0 \end{Bmatrix}$$

2. Test equilibrium angles of attack designated by $\{ \alpha \}$ in degrees.

3. Test equilibrium loads designated by $\{ P_Z \}$ in pounds.

Test Condition	C_{L_F}/C_{L_R} $\{P_{Z_o}\}_1$	$\{P_{Z_o}\}_2$	$\{P_{Z_o}\}_3$
	q = 4 psi		
R. T.	1.556	1.567	1.580
Thermal A	1.630	1.651	1.662
Thermal B	1.716	1.721	1.740
	q = 6 psi		
R. T.	1.926	1.990	2.022
Thermal A	2.088	2.390	2.126
Thermal B	2.130	2.220	2.330
	q = 8 psi		
R. T.	2.540	2.700	2.500
Thermal A	2.492	2.667	2.761
Thermal B	2.570	2.849	3.079

parameters and the temperature effects, a large number of tests (27) on the rectangular specimen were performed.

Variations of the aerodynamic parameters q and α_g are accomplished through variation of the aerodynamic coefficients $\left\{P_{Z_o}\right\}$, $\lfloor \bar{Q}_1 \rceil$ and $\lfloor \bar{Q}_2 \rceil$. Equation (2.14) shows that:

$$\left\{P_{Z_o}\right\} = q \lfloor R \rceil \left\{\left(\frac{\Delta p}{q}\right)_o\right\}$$

$$\lfloor \bar{Q}_1 \rceil = q \lfloor R \rceil \lfloor Q_1 \rceil$$

$$\lfloor \bar{Q}_2 \rceil = q \lfloor R \rceil \lfloor Q_2 \rceil \tag{2.14a}$$

Different values of q can be simulated by simply ratioing the values of the aerodynamic coefficients to certain initial values. As previously described, the "effective" angle of attack is varied by simply changing the initial loads $\left\{P_{Z_o}\right\}$. Initial loads were imposed on the rectangular specimen at points 1, 5, and 9, and on the delta specimen at points 1, 5, 8, and 10. The aerodynamic coefficients listed in Tables 3.1 and 3.2 were obtained using the above procedure. The initial aerodynamic coefficients were determined as part of the preliminary static aeroelastic analyses performed for specimen design purposes.

Nine room temperature tests of the rectangular model were conducted, followed by eighteen elevated temperature tests. The desired temperature distributions were intended to possess a significantly nonlinear chordwise profile while being maintained constant in the spanwise direction and across the specimen thickness. Such profiles are to be anticipated for thin surfaces in sustained hypersonic flight. (The spanwise profile under practical conditions is, of course, disrupted by the presence of the body. These effects are a unique function of the wing and body geometrics and were therefore excluded from the present tests.)

Figure 3.6 illustrates the two chordwise temperature profiles which were imposed on the rectangular specimen. Each of these was continually reproduced for the nine flight conditions. Prior to the imposition of loads for a given flight

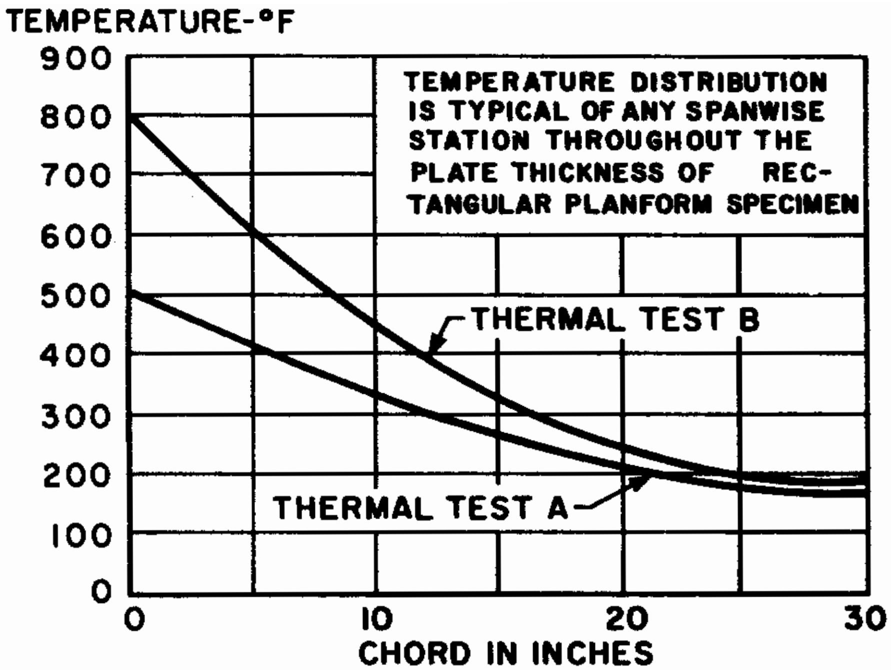

Figure 3.6 Chordwise Temperature Distributions

condition, the desired temperature profile would be established using procedures described earlier. Thermocouples affixed to the specimen verified that there were negligible gradients across the specimen thickness and only minor nonuniformities in the vicinity of the support.

Results from all tests performed, in terms of equilibrium loads and angles of attack, are presented in Tables 3.1 and 3.2. Results of special interest are graph-graphically portrayed in Figures 3.7 and 3.8. The following discussion will be limited to the latter.

A convenient means of portraying the aggregate effect of the equilibrium loads is to compute from them the total flexible load on the wing P_{Z_F} and then form a ratio with the calculated values of the total initial (rigid) load, P_{Z_R}. This ratio, P_{Z_F}/P_{Z_R}, is identical in value to the more familiar ratio of the flexible to rigid lift coefficients, C_{L_F}/C_{L_R}. The required operations were performed on the data shown in Table 3.2 and the results are plotted in Figure 3.7.

In order to introduce thermal effects into the representation shown in Figure 3.7, it was necessary to define a parameter representative of these effects and to compute it for each of the test conditions. The parameter chosen, Φ, is defined as:

$$\Phi = 1 - \frac{E_T}{E_o} \left(1 + \frac{6(1+\nu) \int \sigma_t (c/2-x)^2 \, dx}{E_T \, c t^2} \right) \tag{3.3}$$

where E_T and E_o are the moduli of elasticity at the average temperature of the specimen and at ambient temperature, respectively, and σ_t is the spanwise thermal stress at a chordwise cross section as calculated from thermoelastic beam theory, Φ is a parameter representing the loss in torsional stiffness due to thermal effects; its theoretical basis is developed in detail in Reference 24. It is the ratio between the torsional stiffness at room temperature and the torsional stiffness in the presence of a chordwise temperature gradient and includes the effect of temperature dependent material properties, but excludes the effects of aspect ratio, support conditions, large displacements, and flexural stiffness loss due to thermal effects. Nevertheless, it would appear to be the most applicable simple parameter for graphical representation purposes.

Returning to Figure 3.7a, significant increases in C_{L_F}/C_{L_R} with increases in q and Φ were obtained. Study of these data shows that the loss of torsional stiffness (through increasing Φ) and the increase in dynamic pressure are approximately equally important in determining the rate of change of C_{L_F}/C_{L_R} with these parameters. The test data shown in Figure 3.7b display the effect of variable $\left\{\alpha_g\right\}$ and Φ on C_{L_F}/C_{L_R} for q = 4 psi.

Still another representation of interest is that which shows the variation of the equilibrium angle of attack along the tip chord reference points 9 through 12. Figure 3.8a displays the variation of the angular deformation at reference point 9, α_9. Large increases in the deformation at this point are obtained as structural nonlinearities become more prominent and the magnitude of the aerodynamic nonlinearities are increased through q. Additional selected test results are shown in Figure 3.8b. Significant changes in the equilibrium angle of attack are obtained.

It is concluded that a laboratory technique for the simulation of nonlinear static aerothermoelastic behavior has been successfully demonstrated. In view of the many large scale elevated temperature structural test facilities presently available and the relatively modest proportions of proposed hypersonic configurations, it would appear that the technique is directly useful not only for research, but also for prototype investigations. Results of the tests performed indicate that the effects of the interaction between structural and aerodynamic nonlinearities are indeed significant.

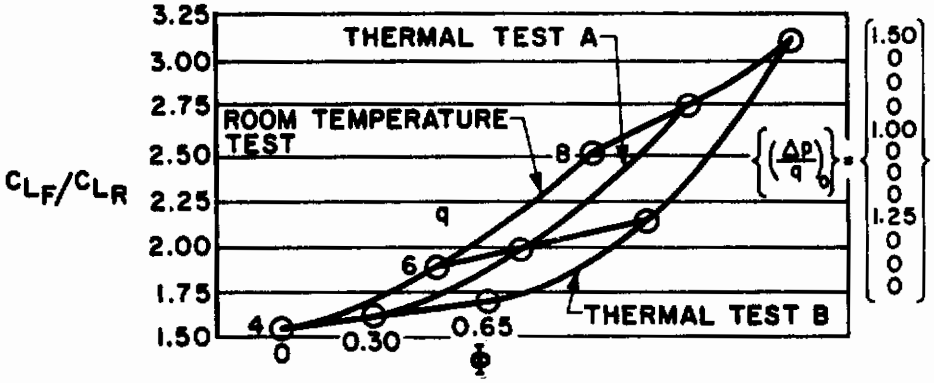

Figure 3.7a. C_{L_F}/C_{L_R} Versus Φ and q

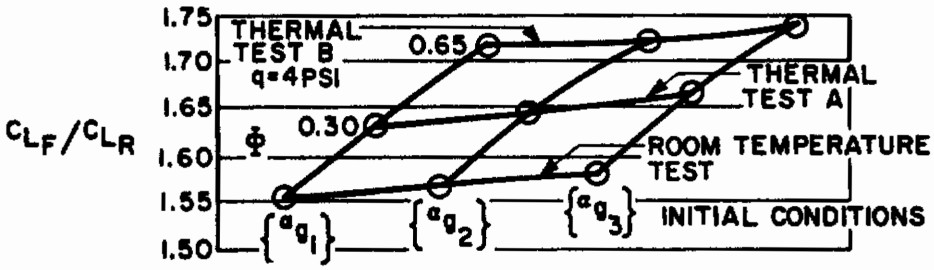

Figure 3.7b. C_{L_F}/C_{L_R} Versus Φ and $\{\alpha_g\}$

Figure 3.7. Integrated Test Results, Rectangular Planform

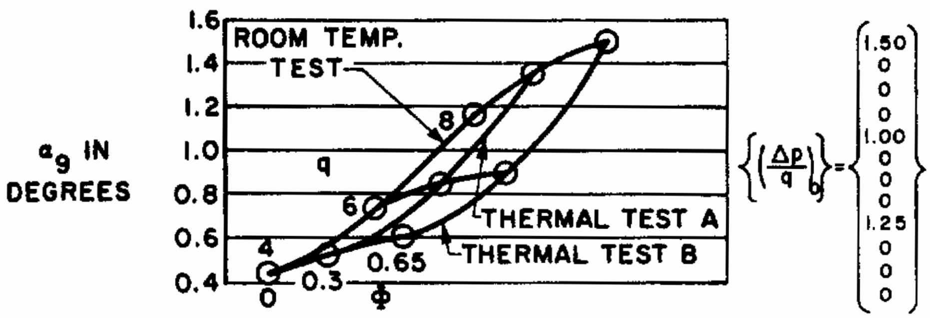

Figure 3.8a. α_g Versus Φ and q

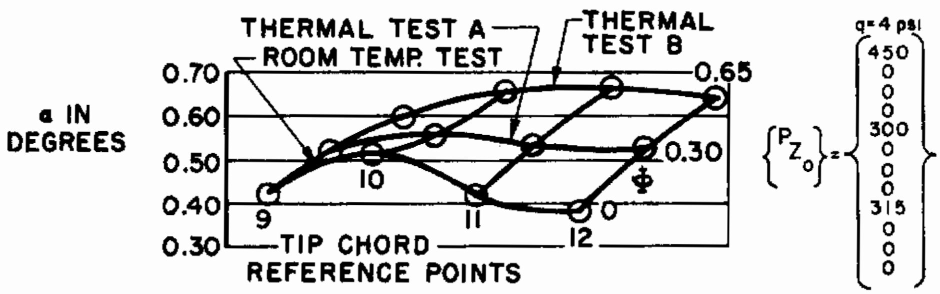

Figure 3.8b. α Versus Φ and Reference Point Position

Figure 3.8. Selected Test Results, Rectangular Planform

SECTION 4.0

THEORY-TEST COMPARISONS

4.1 GENERAL

The objectives of the subject study program, as described in Section 1.0, included the development of an analytical method and related computer program for the analysis of stat'c aeroelastic behavoir and comparisons of the results of such analyses with test data of the previous section. Analyses were restricted to the rectangular planform specimen since only preliminary test results are available for the delta planform specimen. Rectangular planform analyses were conducted at both room and elevated temperatures for several values of the dynamic pressure. Both linear and nonlinear structural behavior in combination with nonlinear aerodynamic behavior was considered. The analyses performed demonstrated the versatility of the computer program and the types and characteristics of solutions available.

4.2 INPUT DATA

Input to the computer program consists of structural and aerodynamic analysis data, respectively. Two major options are available in connection with the structural analysis portion of the program: (1) the basic material property, geometric and temperature data is given so that the computer automatically develops the set of structural influence coefficients; or (2) the structural influence coefficients are provided as input. In the case of option (1), the input specifically consists of the coordinates of the reference points, the type and location of the discrete elements of the structural idealization, material properties, temperatures, boundary conditions, and initial displacements. The structural analysis input also includes a specification of a convergence criterion and the number of iterations allowed for convergence before the program will stop.

Aerodynamic input consists of sets of matrices defining aerodynamic influence coefficients, initial angle of attack distributions, assigned reference point areas, wing geometric properties and numerical integration techniques. Codes in this portion of the input control output format, convergence criterion on $\left\{ \alpha \right\}$, allowable number of iterations, choice of solution type, and correspondence between the aerodynamic and structural reference points.

Figure 3.5a shows reference point location, assigned areas, planform dimensions and the coordinate system for the tested wing specimen. Thirty node points, defining twenty rectangular plate elements, were selected to analytically describe structural behavior. Points 1-6 are located along the root chord; point 1 at the leading edge and point 6 at the trailing edge. This node point distribution is repeated at each spanwise reference point station including the tip station as shown in Figure 4.1. Rectangular plate elements are designated by the corner node points in counterclockwise order. Thus, for example, structural element No. 1 is bounded by node points 1, 2, 8, and 7. The material properties and temperatures associated with each structural element are based on the experimental data of Section 3.0. For the analyses being considered, the initial loads (both in-plane and out-of-plane), initial displacements and thermal moments are zero. Boundary conditions associated with the analyses are specified by assigning zero linear and angular displacements to the root node points.

Aerodynamic influence coefficient matrices are formulated in the manner discussed in Section 3.0 and are proportional to those coefficients given in Table 3.2. The initial angle of attack distributions for the planform under study are zero since the specimen remained horizontal during test and in addition had no built in camber or twist. The assigned reference point areas and wing geometric properties are easily obtained from Figure 3.5a. Integration matrices normally used in aeroelastic analyses (See Reference 22) are replaced by special matrices pertinent to this analysis and are given in Table 4.1. As previously mentioned, thirty structural node points were specified. Twelve of these correspond to aerodynamic reference points; thus, a distinction between these sets of points must be made. This is accomplished by listing, as program input, those points which are not common to the aerodynamic-aeroelastic analysis.

The analysis method of Section 2.0 stipulates that either the closed form or series type solution may be used to obtain the equilibrium angles of attack. In the subject analyses, Equations (2.21) and (2.22) were used and solutions are designated by types m = 0 and m = 1, respectively. The closed form solution cannot be used in the present case since the initial angles of attack, $\tilde{\alpha}_g$, are zero. Input matrices for the subject analyses are given in Table 4.1.

4.3 DISCUSSION OF RESULTS

4.3.1 Slope Influence Coefficient Matrices

Use will be made of experimentally determined as well as theoretically derived slope influence coefficients in the theory-test comparisons to be described in the next section. Hence, it is of importance to examine and compare these theoretical and test values.

Two solution approaches were taken to determine the analytical slope influence coefficients. First, the finite difference scheme advanced by Williams (Reference 29) was employed in analyses predating the checkout of the aeroelasticity computer program. The scheme of Reference 29 leads directly to influence coefficients for the lateral displacements; these values were then numerically differentiated to obtain the slope influence coefficients. A relatively fine gridwork of 54 points was used in the development of these results.

In the other approach, the plate discrete element relationships developed in connection with the computer program of this study were utilized. Such relationships lead directly to the slope influence coefficients. The gridwork shown in Figure 4.1 was employed.

Three comparisons of these results appear in Figures 4.2 through 4.4. In Figures 4.2 and 4.3, the test results are compared with the results of the finite difference (Reference 29) and discrete element approaches, respectively. It is to be noted that these sets of influence coefficients are not symmetric. An entire set of displacement influence coefficients relating the applied forces and moments to the linear and rotational displacements is symmetric, as indicated in the equation below. The portion of such a master matrix relating the vertical loads (P_z) to the chordwise angular displacements (α_y) (i.e., the slope influence coefficient matrix $\left[\delta_{\alpha_z}\right]$) is shown crosshatched. It is apparent that no fundamental requirements of symmetry apply to this portion of the complete matrix.

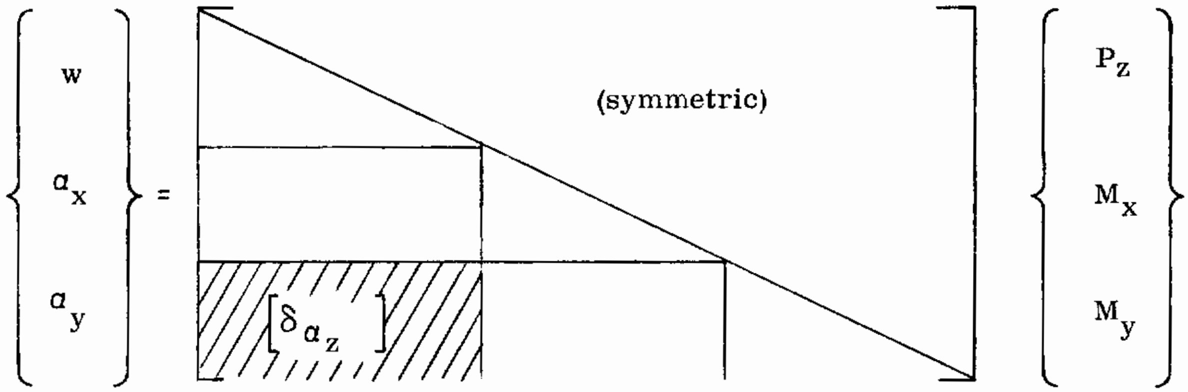

(4.1)

An additional comparison is provided in Figure 4.4, wherein both analytical derived sets of influence coefficients are tabulated. In general, there is a relatively close agreement between the two sets in view of the further analytical approximations introduced by the numerical differentiation procedures applied to the results of the finite difference approach. The discrete element results are to be preferred by virtue of the sophistication of the element relationships as compared with the displacement idealization concepts of the finite difference approach.

Returning now to the comparisons of theory and test, it is seen from Figures 4.2 and 4.3 that there exists an erratic degree of correspondence between the results for the different influence coefficients. The theoretical and test values of points along the tip (points 9-12) differ in the range of +15 to -15%, with certain values being in very close agreement. Percentage wise, differences for points near the root are very much greater, but the absolute values at these points are relatively small and test results are unreliable in these regions. It is pertinent to note that, in nearly all cases, both analytical values of an influence coefficient are on the same side of the test result; i.e., they either are both too stiff or too flexible. Furthermore, with the prevalence of negative influence coefficients, all analytical values are found to be of the same sign as the test results.

These comparisons indicate the possibility of either measurement errors in the test data or the presence of root flexibility effects (support displacements) that are not accounted for in the analyses, or a combination of the two circumstances. Since it had not been anticipated that experimental influence coefficients would play a rôle in the interpretation of the aeroelastic theory-test comparisons, the measurements were not taken with the care demanded of searching theory-test comparisons. As will be seen, however, accurate test results would have proven valuable in this regard and it would have been extremely desirable to define the significance of support flexibility effects.

Nevertheless, it has been indicated that the angular displacement measurement system is capable of providing an acceptable means for the determination of slope influence coefficients. More accurate and reliable results would appear feasible if careful test procedures are adhered to. It was not possible to define the significance of root flexibility effects in the tests conducted.

4.3.2 Aeroelastic Theory-Test Comparisons – Room Temperature Conditions

Results of room temperature aeroelastic analyses are shown in Table 4.2 and in Figures 4.5 to 4.7. Analyses designated as type "I", representing solutions achieved prior to checkout of the automatic structural analysis features of the complete computer program, utilized slope influence coefficients based on the finite difference scheme of Reference 29. (See previous section.) Analyses designated as types "II" and "III" are based entirely on use of the discrete element method of linear structural analysis and the related computer program discussed in Section 2.0. Test data are shown by the various symbols.

Figure 4.5 shows a comparison between the test data and the results of Type I aeroelastic analyses. Although the level of agreement is remarkably close, it is to be remembered that the structural input to this analysis did not agree with the corresponding test data to the same extent (see previous section). Also, the stiffening effects of large deflections are not included in the analysis. These two factors should be compensatory since the structural analysis is deficient in predicting root flexibility effects.

Further comparisons between test data and the results of analyses appear in Figure 4.6. Type II analyses involve linear representations of the structural behavior. Type III analyses also involve linear representations of structural behavior but with a modification intended to account for root flexibility effects. Due to the possible influence of root flexibility effects, brought to light by theory-test comparisons of the structural influence coefficients, it was decided to attempt analyses wherein the effective span of the specimen extended to the centerline, rather than to the face of the support. This may be regarded as an extreme representation of root flexibility.

As seen in Figure 4.6, both the basic linear analysis and the analysis which includes simulation of root flexibility are in approximate agreement with the test data at $q = 4.0$ psi and $q = 6.0$ psi. Since the shape of the test curve is different from that of the analyses, there is an agreement of the Type II analysis results with tests along the rearward portion of the chord while the Type III analysis conforms to test data along the front portion. At $q = 8.0$ psi the Type II analysis is generally in closer conformity with the test data.

The analytical results of Figure 4.6 disregard, of course, the existence of nonlinear (large deflection) effects. Such effects appear in the results of the Type IV and V analyses, as shown in Figure 4.7. Only the $q = 8.0$ psi case was examined since the displacements of the $q = 4.0$ and 6.0 psi conditions do not appear large enough to introduce significant nonlinear effects. (At $q = 8$ psi the measured tip deflection was 4.65 times the plate thickness.) The Type IV analysis is the counterpart of the linear analysis (Type II) described above. The Type V analysis corresponds to the analysis which attempted to account for root flexibility effects (Type III). It is seen from Figure 4.7 that the Type IV analysis with inclusion of nonlinear effects, has moved the linear solution away from the test data. On the other hand, the nonlinear analysis, with inclusion of root flexibility effects (Type V), demonstrates a good degree of correspondence with the test results. As pointed out in the previous section, theory-test comparisons of structural influence coefficients supported the view that root flexibility effects were indeed significant.

In summary, it is seen that for this study, where special attention was given to designing a wing specimen with large elastic deflections, the effects of "large deflections" were not severe at room temperature. A nonlinear analysis, which included an estimate of root flexibility effects (Type V), yielded results which were in reasonable agreement with the test data.

A few comments on solution type and convergence of $\left\{ \alpha \right\}$ are in order. The lower portion of Table 4.3 lists the number of iterations performed to obtain convergence using type m = 0 and m = 1 solutions and the approximate machine time for each solution type. In all cases except one, type m = 0 required a smaller number of iterations than type m = 1. In some instances type m = 1 did not converge after 25 iterations (indicated by NC). Values of the equilibrium angle of attack, using either solution type, agreed within 4%, the small error being attributed to the convergence criterion used. Approximate machine time for type m = 0 is very small indicating an efficient computational program. Consideration of structural nonlinearities complicates the solution process to a great degree and this is reflected in the number of iterations and associated computer time. Analysis IV, type m = 0, took six minor $\left\{ \alpha \right\}$, six minor $\left[\delta_{\alpha_z} \right]$ and seven major $\left\{ \alpha \right\}$ iteration loops to obtain convergence. Total time for this analysis was approximately 35 minutes, an extremely large amount of time in comparison to analyses I, II and III.

4.3.3 Aeroelastic Theory-Test Comparisons – Elevated Temperature Conditions

The imposition of elevated temperatures on the test specimen introduces deterioration of the modulus of elasticity and a change in the deflectional stiffness produced by the presence of midplane stresses due to thermal gradients.

These phenomena produced major changes in the stiffness of the specimen; in the case of thermal test A, the conditions at $q = 8$ psi produced a tip deflection 5.75 times the specimen thickness. Similarly, the conditions associated with $q = 8$ psi, thermal test B, produced a ratio of tip deflection to specimen thickness of 7.0.

It is of interest to note that in the approximate analyses of Section 3.3, the estimated stiffness losses due to material property degradation were 6 and 8%, respectively, for thermal tests A and B. Also, the torsional stiffness losses were estimated as 30 and 65%, respectively. Hence, it is to be expected that midplane stresses due to large deflections had a considerable influence on the flexibility of the model under the subject elevated temperature conditions.

It was intended that the analyses for elevated temperature conditions be performed in two phases. First, measured equilibrium test loads were to be combined with computed (linear) structural influence coefficients. (The computation of these influence coefficients is discussed below.) The results of these analyses are designated as Types VI and VII. The intended second group of analyses were to be conducted with the inclusion of structural as well as aerodynamic nonlinearities. It was anticipated that, with the results of these types of analyses, it would be possible to isolate the influence of the various effects of temperature and large deflections on the equilibrium displacements. Only one attempt at effecting a completely nonlinear solution to the problem (designated by Type VIII) met with success, however, due to lack of convergence in the iterative portions of the structural analysis procedures. Since it was not possible to resolve these difficulties within the period of the study program, the only other test-theory comparisons available are those related to analyses types VI and VII. It is believed that the source of difficulty in obtaining a convergent solution for structural behavior can be resolved by developments which are outlined in Section 5.0.

Linear structural analyses performed with the use of the computer program indicated relatively severe deflectional behavior. The values thus derived appeared to be unreliable in certain regions of the structure, indicating possible conditions of local instability in these regions. Hence, an alternate structural analysis computer program was employed. This program, described in Reference 30, is based on the same concepts as the present program but employs more sophisticated relationships in the definition of the temperature state and in the determination of the influence of the in-plane thermal stresses on deflectional behavior.

As noted earlier, two types of analyses were performed with this linear structural representation. Results of these analyses are shown in Figures 4.8 and 4.9. Figure 4.8 represents comparisons wherein only the stiffness reducing effect of the elastic modulus change due to temperature is taken into account (i.e., analysis Type VI). In Figure 4.9, both the elastic modulus change and thermal stress effects are included in the analytical results designated by the numeral VII.

It is seen from Figure 4.8 that the effects of temperature environment on the modulus change are not significant. On the other hand, the thermal stress effects as defined in Figure 4.9 are extremely severe. Evidently, the large deflection effects are of significance since these must account for the major share of the discrepancies between theory and test.

The single nonlinear aerothermoelastic solution achieved is compared with test data in Figure 4.10. This solution was effected for the case of $q = 8.0$ psi, thermal test B. The results are seen to be in remarkable agreement with the test data for the points near the trailing edge. There is a considerable difference between theory and test for the leading edge point, however. It is noteworthy that the same type of discrepancy was recorded at the leading edge points for the analyses of room temperature conditions. Of interest also is the increase in computer time for the subject heated wing aeroelastic analyses in comparison to the analogous room temperature analyses. (See Tables 4.2 and 4.3.)

It is seen that for elevated temperatures, the test specimen sustained major changes in stiffness resulting in significant large deflection effects. Attempts to predict these effects in combination with nonlinear aerodynamic behavior have met with partial success. It is evident that additional test work and analytical comparisons are necessary.

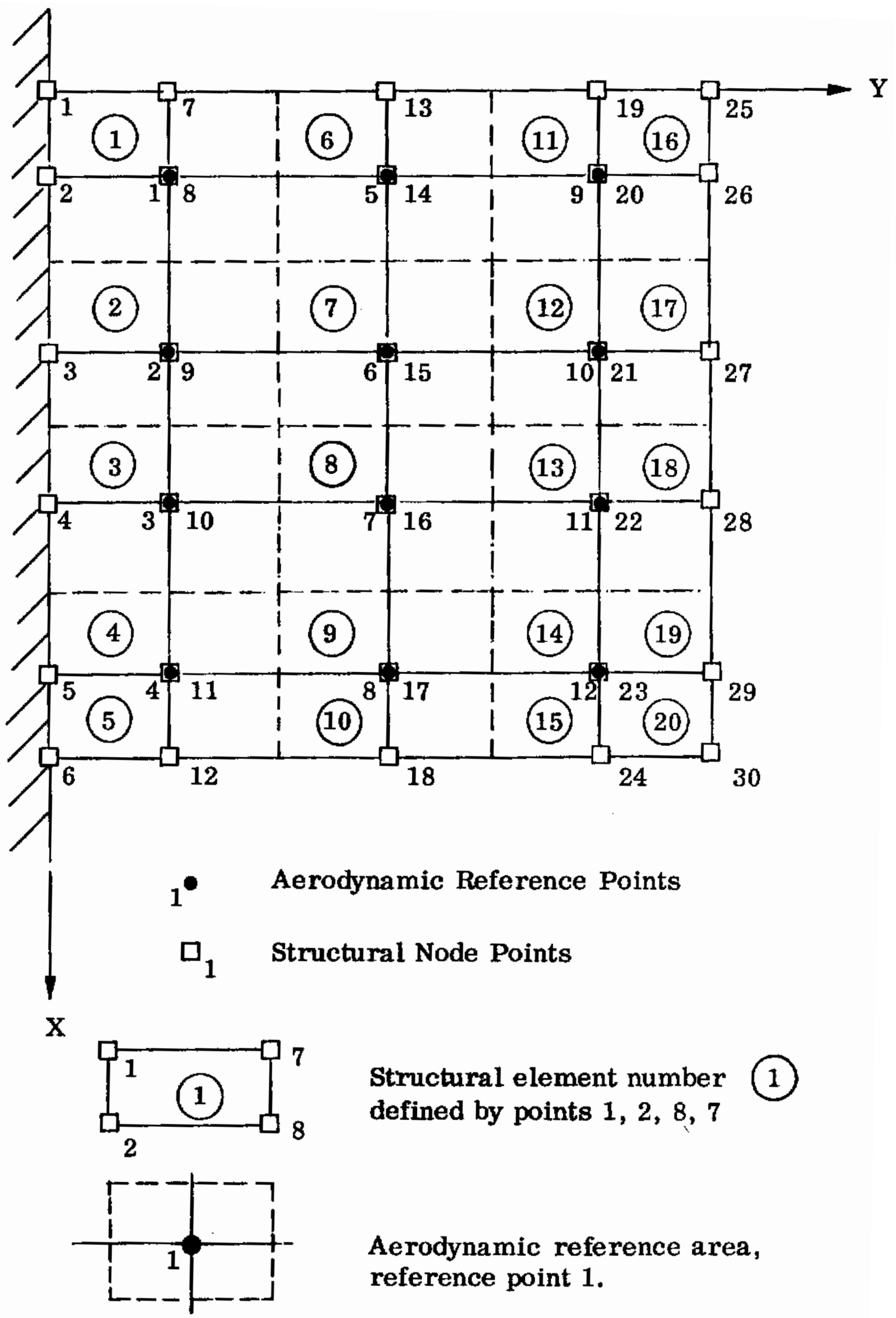

Figure 4.1. Rectangular Planform Reference Points

α_{12}		-9.7277*	0.2167	5.2973	8.7651	-5.5872	-0.4335	2.6008	4.4313	-1.0692	-0.0957	0.4380	0.7884	$P_{Z_{12}}$
		-11.9221**	-0.7320	3.4874	5.5929	-6.0494	-0.6333	1.9856	3.4656	-1.2050	-0.1028	0.4796	0.7681	
α_{11}		-10.5016	-2.3335	5.0418	9.4667	-5.5502	-1.3681	2.3127	4.9289	-1.0331	-0.2420	0.3937	0.8958	$P_{Z_{11}}$
		-10.6558	-2.6805	3.6056	6.5942	-5.7657	-1.5757	1.8694	4.1047	-1.1564	-0.2839	0.4326	1.0148	
α_{10}		-9.4667	-5.0418	2.3335	10.5016	-4.9289	-2.3127	1.3681	5.5502	-0.8958	-0.3937	0.2420	1.0331	$P_{Z_{10}}$
		-8.6443	-3.9213	1.8946	8.1373	-4.8593	-2.3181	1.0616	4.7312	-1.0124	-0.5062	0.1968	1.0385	
α_9		-8.7651	-5.2973	-0.2167	9.7277	-4.4313	-2.6008	0.4335	5.5872	-0.7884	-0.4380	0.0957	1.0692	P_{Z_9}
		-6.5044	-3.1526	0.7252	8.7031	-3.7864	-2.1898	0.4266	4.8068	-0.8263	-0.4977	0.0559	1.0329	
α_8		-4.3825	0.6502	3.9003	5.7317	-4.9126	0.4335	2.1908	3.1309	-1.0493	0.0966	0.4624	0.5969	P_{Z_8}
		-6.2681	-0.4747	2.2442	3.5206	-5.0844	0.3596	1.8202	2.4456	-1.1859	0.1439	0.5311	0.5703	
α_7		-5.2332	-1.0837	2.6062	5.1700	-4.3482	-0.8498	2.1375	3.4000	-0.9870	-0.1770	0.4624	0.7152	P_{Z_7}
		-6.6066	-1.8184	1.5657	2.6583	-5.0367	-1.1080	1.9626	2.9492	-1.2033	-0.2175	0.5815	0.7518	
α_6	$= 10^{-6}$	-5.1700	-2.6062	1.0837	5.2332	-3.4000	-2.1375	0.8498	4.3482	-0.7152	-0.4624	0.1770	0.9870	P_{Z_6}
		-4.8077	-1.8263	1.3135	4.7863	-3.4609	-2.1974	0.8538	2.3980	-0.8465	-0.5700	0.1966	0.9984	
α_5		-5.7317	-3.9003	-0.6502	4.3825	-3.1309	-2.1908	-0.4335	4.9126	-0.5969	-0.4624	-0.0966	1.0593	P_{Z_5}
		-3.7076	-1.7111	0.7523	4.8574	-2.5300	-1.8931	-0.3617	4.0002	-0.6221	-0.5353	-0.2067	1.0482	
α_4		-0.1924	0.6214	1.3483	1.6183	-0.7703	0.3368	0.7035	0.8859	-0.6836	0.3946	0.2312	0.1634	P_{Z_4}
		-1.0870	0.1863	0.7972	1.0146	-1.1438	0.3271	0.6578	0.7247	-0.6522	0.4348	0.2588	0.1449	
α_3		-0.9058	-0.1607	0.4867	0.9518	-0.9184	-0.1680	0.4768	0.7116	-0.6285	-0.0477	0.4362	0.2384	P_{Z_3}
		-1.4373	-0.4736	0.1350	0.5296	-1.1631	-0.2908	0.4362	0.6215	-0.6858	-0.1454	0.4933	0.2891	
α_2		-0.9518	-0.4867	0.1607	0.9058	-0.7116	-0.4768	0.1680	0.9184	-0.2384	-0.4362	0.0477	0.6285	P_{Z_2}
		-0.8696	-0.2899	0.3679	0.9755	-0.7620	-0.5073	0.1760	1.0146	-0.2899	-0.4928	0.1346	0.4400	
α_1		-1.6183	-1.3483	-0.6214	0.1924	-0.8859	-0.7035	-0.3368	0.7703	-0.1634	-0.2312	-0.3946	0.6836	P_{Z_1}
		-0.6980	-0.2025	0.4362	1.4436	-0.6190	-0.4798	-0.0779	1.2141	-0.1973	-0.2908	-0.4258	0.6817	

* Theoretical Values, Reference 29
** Test Values

Figure 4.2. Theory-Test Comparisons, Rectangular Planform Room Temperature Slope Influence Coefficients

α_{12}		-9.6600*	0.6810	5.9700	9.2600	-5.6900	-0.3660	2.7900	4.6000	-0.9620	-0.0964	0.4340	0.7360	$P_{Z_{12}}$
		-11.9221**	-0.7320	3.4874	5.5929	-6.0494	-0.6333	1.9856	3.4656	-1.2050	-0.1028	0.4796	0.7681	
α_{11}		-10.7000	-2.2700	5.3300	9.8100	-5.5100	-1.2900	2.3500	5.0500	-0.8980	-0.1970	0.3350	0.8170	$P_{Z_{11}}$
		-10.6558	-2.6805	3.6056	6.5942	-5.7657	-1.5757	1.8694	4.1047	-1.1564	-0.2839	0.4326	1.0148	
α_{10}		-9.8100	-5.3300	2.2700	10.7000	-5.0500	-2.3500	1.2900	5.5100	-0.8170	-0.3350	0.1970	0.8980	$P_{Z_{10}}$
		-8.6443	-3.9213	1.8946	8.1373	-4.8593	-2.3181	1.0616	4.7312	-1.0124	-0.5062	0.1968	1.0385	
α_9		-9.2600	-5.9700	-0.6810	9.6600	-4.6000	-2.7900	0.3660	5.6900	-0.7360	-0.4340	0.0964	0.9620	P_{Z_9}
		-6.5044	-3.1526	0.7252	8.7031	-3.7864	-2.1898	0.4266	4.8068	-0.8263	-0.4977	0.0559	1.0329	
α_8		-4.2800	1.0500	4.2600	6.0800	-4.0400	0.9070	2.3900	3.1700	-0.9380	0.2070	0.4660	0.5100	P_{Z_8}
		-6.2681	-0.4747	2.2442	3.5206	-5.0844	0.3596	1.8202	2.4456	-1.1859	0.1439	0.5311	0.5703	
α_7	$= 10^{-6}$	-5.2000	-1.0200	2.6500	5.3200	-4.4000	-0.7700	2.3200	3.3400	-0.8580	-0.1350	0.4360	0.6530	P_{Z_7}
		-6.6066	-1.8184	1.5657	2.6583	-5.0367	-1.1080	1.9626	2.9492	-1.2033	-0.2175	0.5815	0.7518	
α_6		-5.3200	-2.6500	1.0200	5.2000	-3.3400	-2.3200	0.7700	4.4400	-0.6530	-0.4360	0.1350	0.8580	P_{Z_6}
		-4.8077	-1.8263	1.3135	4.7863	-3.4609	-2.1974	0.8538	2.3980	-0.8465	-0.5700	0.1966	0.9984	
α_5		-6.0800	-4.2600	-1.0500	4.2800	-3.1700	-2.3900	0.9070	4.0400	-0.5100	-0.4660	-0.2070	0.9380	P_{Z_5}
		-3.7076	-1.7111	0.7523	4.8574	-2.5300	-1.8931	-0.3617	4.0002	-0.6221	-0.5353	-0.2067	1.0482	
α_4		-0.2420	0.6640	1.2700	1.5700	-0.7580	0.4560	0.7690	0.8000	-0.2583	0.4830	0.1090	0.1200	P_{Z_4}
		-1.0870	0.1863	0.7972	1.0146	-1.1438	0.3271	0.6578	0.7247	-0.6522	0.4348	0.2588	0.1449	
α_3		-0.8910	-0.2370	0.3150	0.7630	-0.8690	-0.1900	0.3960	0.5940	-0.6100	-0.0388	0.4720	0.0782	P_{Z_3}
		-1.4373	-0.4736	0.1350	0.5296	-1.1631	-0.2908	0.4362	0.6215	-0.6858	-0.1454	0.4933	0.2891	
α_2		-0.7630	-0.3150	0.2370	0.8910	-0.5940	-0.3960	0.1900	0.8690	-0.0782	-0.4720	0.0388	0.6100	P_{Z_2}
		-0.8696	-0.2899	0.3679	0.9755	-0.7620	-0.5073	0.1760	1.0146	-0.2899	-0.4928	0.1346	0.4400	
α_1		-1.5700	-1.2700	-0.6640	0.2420	-0.8000	-0.7690	-0.4560	0.7580	-0.1200	-0.1090	-0.4830	0.2583	P_{Z_1}
		-0.6980	-0.2025	0.4362	1.4436	-0.6190	-0.4798	-0.0779	1.2141	-0.1973	-0.2908	-0.4258	0.6817	

* Theoretical Values, Reference 17

** Test Values

Figure 4.3. Theory-Test Comparisons, Rectangular Planform Room Temperature Influence Coefficients

α													P_z
α_{12}	= 10^{-6}	-9.6600*	0.6810	5.9700	9.2600	-5.6900	-0.3660	2.7900	4.6000	-0.9620	-0.0964	0.4340	0.7360
		-9.7277**	0.2167	5.2973	8.7651	-5.5872	-0.4335	2.6008	4.4313	-1.0692	-0.0957	0.4380	0.7884
α_{11}		-10.7000	-2.2700	5.3300	9.8100	-5.5100	-1.2900	2.3500	5.0500	-0.8980	-0.1970	0.3350	0.8170
		-10.5016	-2.3335	5.0418	9.4667	-5.5502	-1.3681	2.3127	4.9289	-1.0331	-0.2420	0.3937	0.8958
α_{10}		-9.8100	-5.3300	2.2700	10.7000	-5.0500	-2.3500	1.2900	5.5100	-0.8170	-0.3350	0.1970	0.8980
		-9.4667	-5.0418	2.3335	10.5016	-4.9289	-2.3127	1.3681	5.5502	-0.8958	-0.3937	0.2420	1.0331
α_9		-9.2600	-5.9700	-0.6810	9.6600	-4.6000	-2.7900	0.3660	5.6900	-0.7360	-0.4340	0.0964	0.9620
		-8.7651	-5.2973	-0.2167	9.7277	-4.4313	-2.6008	0.4335	5.5872	-0.7884	-0.4380	0.0957	1.0692
α_8		-4.2800	1.0500	4.2600	6.0800	-4.0400	0.9070	2.3900	3.1700	-0.9380	0.2070	0.4660	0.5100
		-4.3825	0.6502	3.9003	5.7317	-4.9126	0.4335	2.1908	3.1309	-1.0593	0.0966	0.4624	0.5969
α_7		-5.2000	-1.0200	2.6500	5.3200	-4.4000	-0.7700	2.3200	3.3400	-0.8580	-0.1350	0.4360	0.6530
		-5.2332	-1.0837	2.6062	5.1700	-4.3482	-0.8498	2.1375	3.4000	-0.9870	-0.1770	0.4624	0.7152
α_6		-5.3200	-2.6500	1.0200	5.2000	-3.3400	-2.3200	0.7700	4.4400	-0.6530	-0.4360	0.1350	0.8580
		-5.1700	-2.6062	1.0837	5.2332	-3.4000	-2.1375	0.8498	4.3482	-0.7152	-0.4624	0.1770	0.9870
α_5		-6.0800	-4.2600	-1.0500	4.2800	-3.1700	-2.3900	-0.9070	4.0400	-0.5100	-0.4660	-0.2070	0.9380
		-5.7317	-3.9003	-0.6502	4.3825	-3.1309	-2.1908	-0.4335	4.9126	-0.5969	-0.4624	-0.0966	1.0593
α_4		-0.2420	0.6640	1.2700	1.5700	-0.7580	0.4560	0.7690	0.8000	-0.2583	0.4830	0.1090	0.1200
		-0.1924	0.6214	1.3483	1.6183	-0.7703	0.3368	0.7035	0.8859	-0.6836	0.3946	0.2312	0.1634
α_3		-0.8910	-0.2370	0.3150	0.7630	-0.8690	-0.1900	0.3960	0.5940	-0.6100	-0.0388	0.4720	0.0782
		-0.9058	-0.1607	0.4867	0.9518	-0.9184	-0.1680	0.4768	0.7116	-0.6285	-0.0477	0.4362	0.2384
α_2		-0.7630	-0.3150	0.2370	0.8910	-0.5940	-0.3960	0.1900	0.8690	-0.0782	-0.4720	0.0388	0.6100
		-0.9518	-0.4867	0.1607	0.9058	-0.7116	-0.4768	0.1680	0.9184	-0.2384	-0.4362	0.0477	0.6285
α_1		-1.5700	-1.2700	-0.6640	0.2420	-0.8000	-0.7690	-0.4560	0.7580	-0.1200	-0.1090	-0.4830	0.2583
		-1.6183	-1.3483	-0.6214	0.1924	-0.8859	-0.7035	-0.3368	0.7703	-0.1634	-0.2312	-0.3946	0.6836

	P_z vector
	$P_{Z_{12}}$
	$P_{Z_{11}}$
	$P_{Z_{10}}$
	P_{Z_9}
	P_{Z_8}
	P_{Z_7}
	P_{Z_6}
	P_{Z_5}
	P_{Z_4}
	P_{Z_3}
	P_{Z_2}
	P_{Z_1}

* Theoretical Values, Reference 17
** Theoretical Values, Reference 29

Figure 4.4. Comparison of Theoretical Room Temperature Influence Coefficients, Rectangular Planform

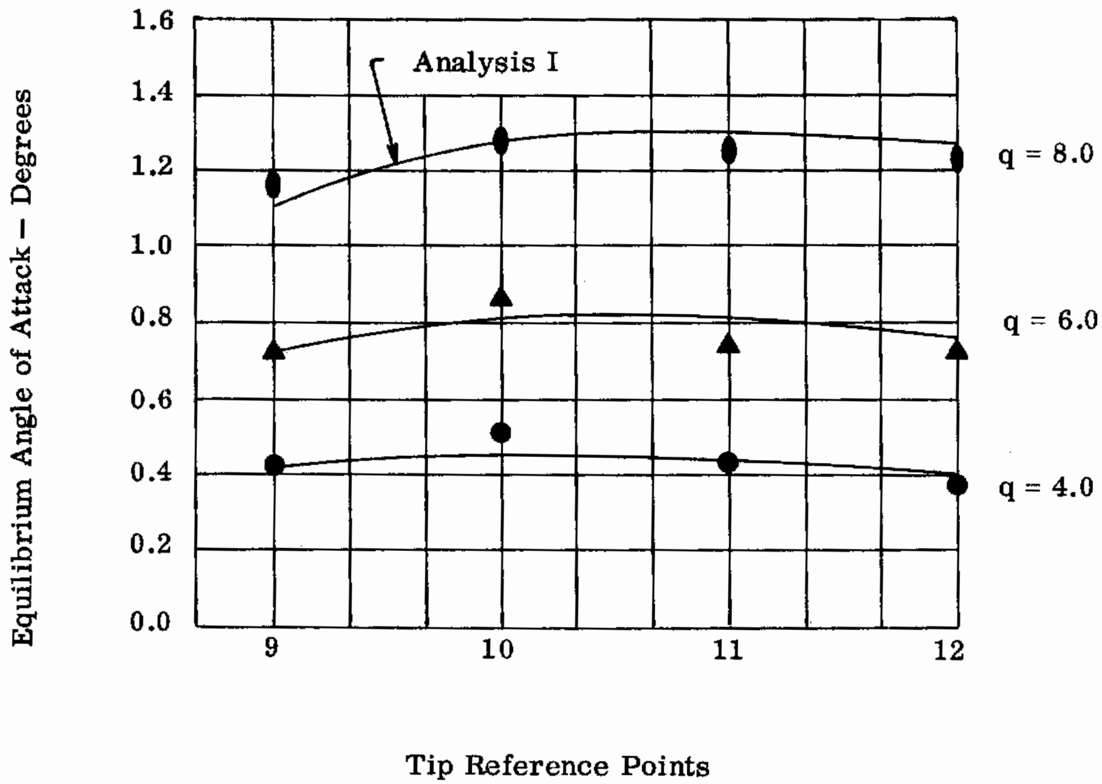

Figure 4.5. Theory-Test Comparisons, Rectangular Planform, Room Temperature

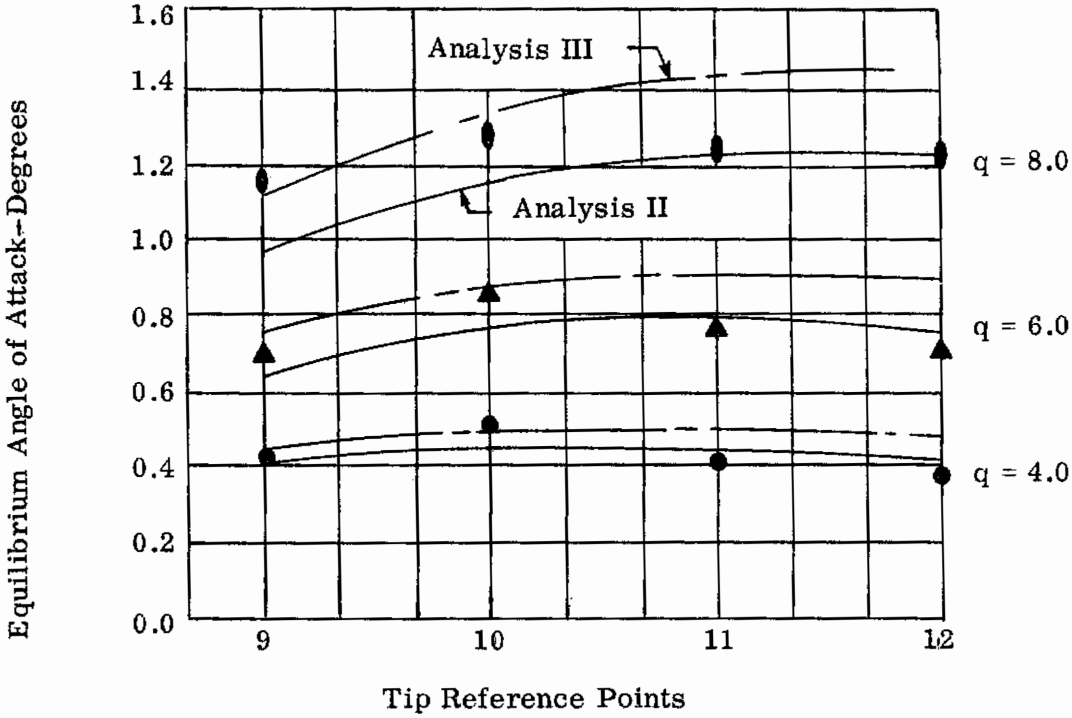

Figure 4.6. Theory-Test Comparisons, Rectangular Planform, Room Temperature

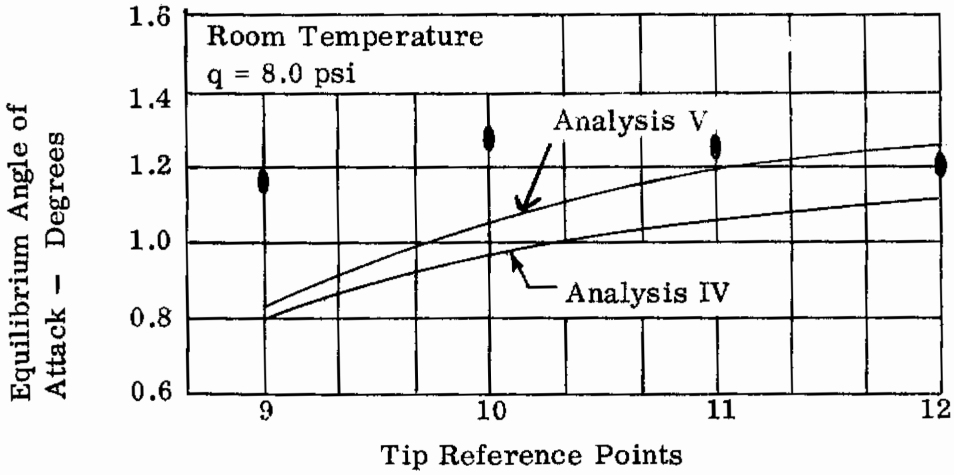

Figure 4.7. Theory-Test Comparisons, Rectangular Planform, Room Temperature

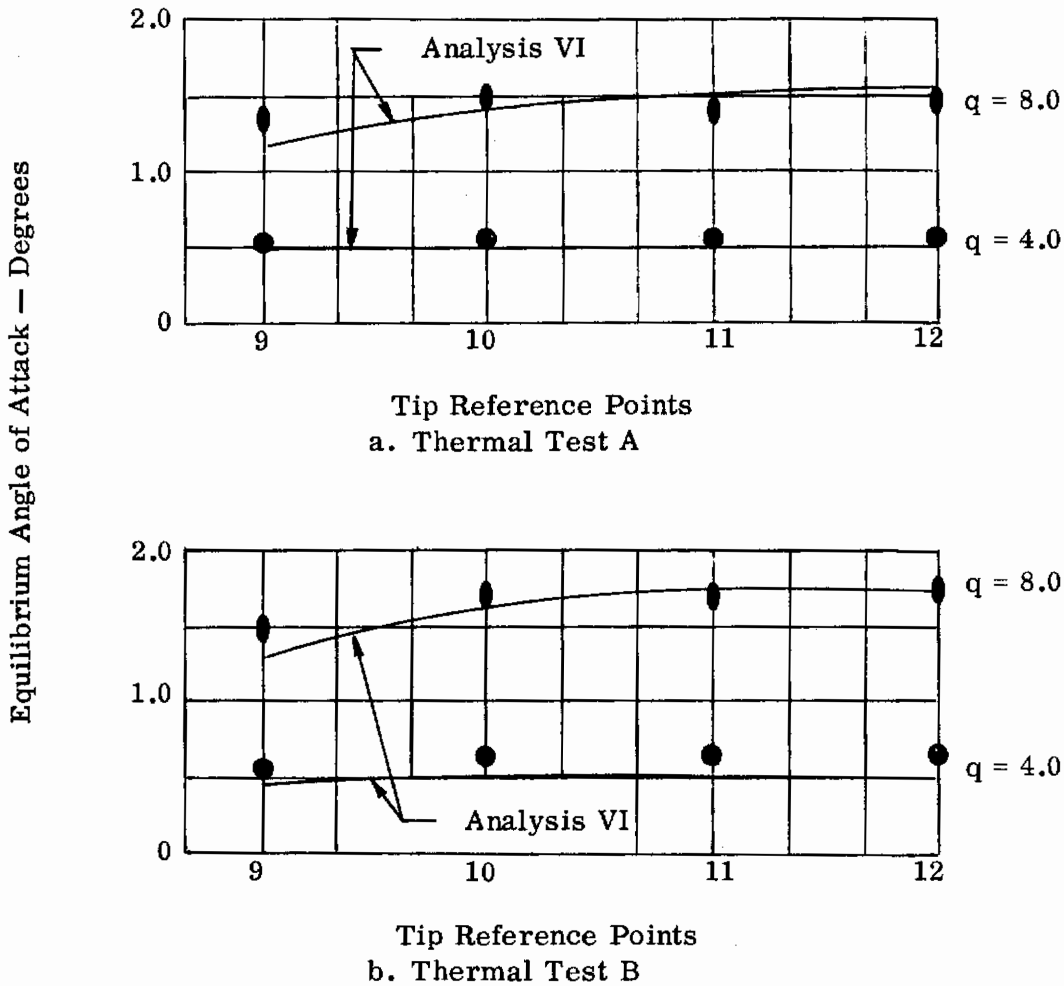

Figure 4.8. Theory-Test Comparisons, Rectangular Planform, Elevated Temperatures

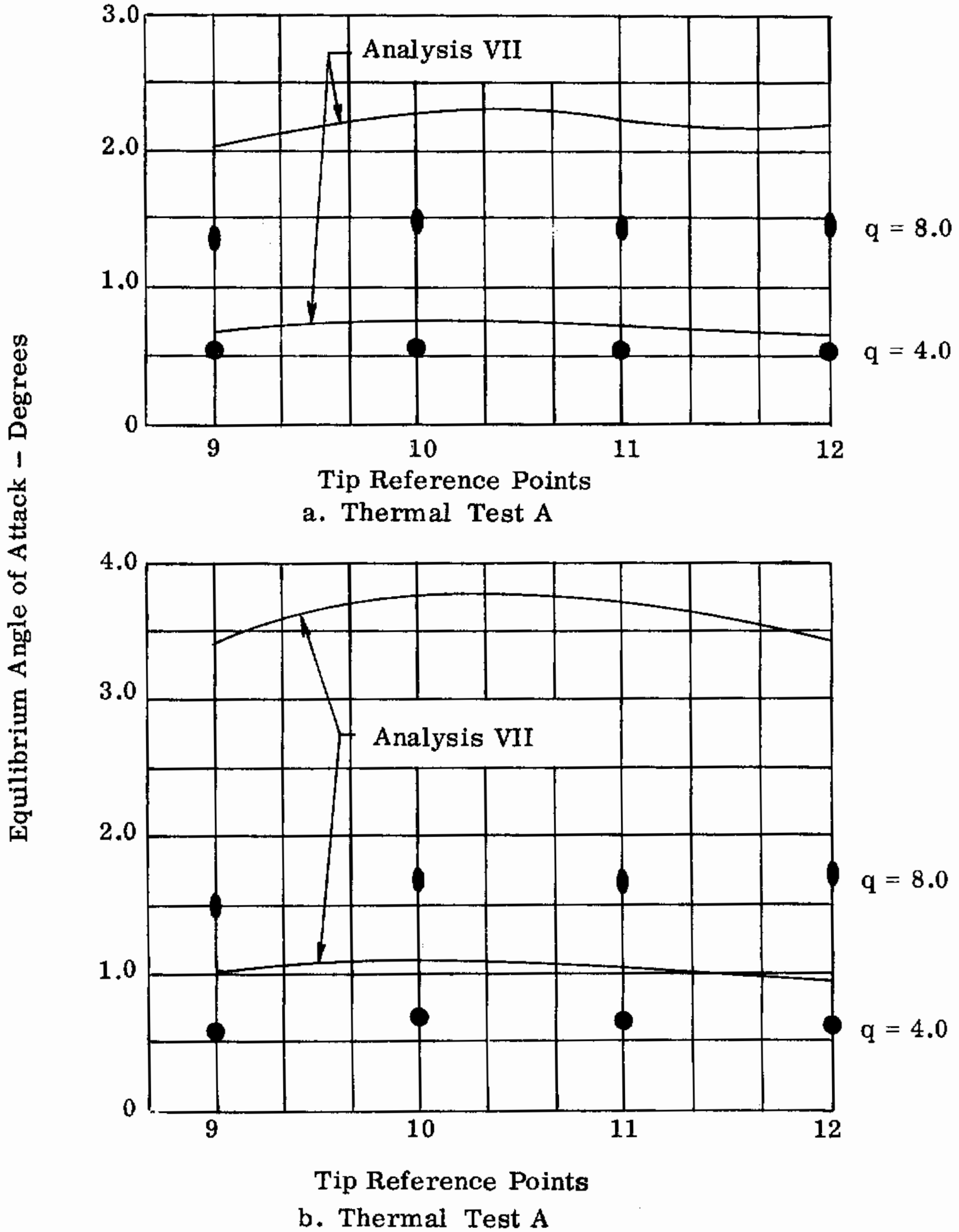

Figure 4.9. Theory - Test Comparisons, Rectangular Planform, Elevated Temperatures

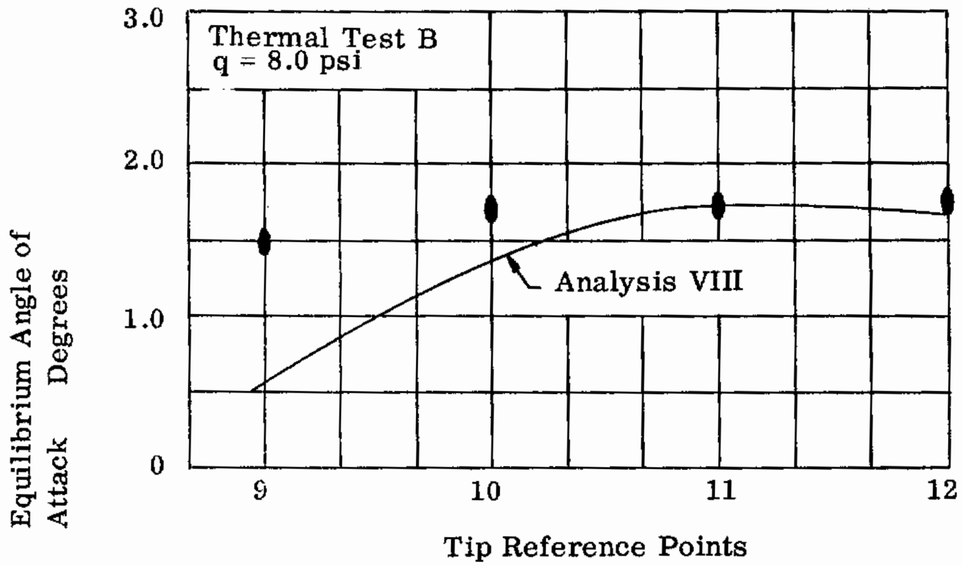

Figure 4.10. Theory-Test Comparisons Rectangular Planform, Thermal Test B

TABLE 4.1

AERODYNAMIC, GEOMETRIC AND INTEGRATION MATRICES

Aerodynamic Matrices					
Reference Point	$\lfloor Q_0 \rceil$	$\lfloor Q_1 \rceil$	$\lfloor Q_2 \rceil$	$\lfloor Q_3 \rceil$	$\{\bar{\alpha}_g\}$
1	1.50	125.0	500.0	0	0
2	0	100.0	350.0	0	0
3	0	50.0	150.0	0	0
4	0	12.5	75.0	0	0
5	1.00	96.0	400.0	0	0
6	0	66.0	300.0	0	0
7	0	24.0	150.0	0	0
8	0	6.0	75.0	0	0
9	1.25	55.0	400.0	0	0
10	0	35.0	300.0	0	0
11	0	15.0	100.0	0	0
12	0	5.0	100.0	0	0
$\lfloor Q_a \rceil = \lfloor 0 \rceil$, $Q_b = 0$; q = 4.0, 6.0, 8.0 psi					

$$\lfloor c/\bar{c} \rceil = \begin{bmatrix} 1.00 & 0 & 0 \\ 0 & 1.00 & 0 \\ 0 & 0 & 1.00 \end{bmatrix}, \quad \lfloor I \rceil = \lfloor 1.0 \quad 1.0 \quad 1.0 \rceil$$

$$\lfloor R \rceil = \lfloor 75.0 \rceil \text{, 30 in. span}$$

$$\lfloor R \rceil = \begin{bmatrix} 82.5 \\ 82.5 \\ 82.5 \\ 82.5 \\ 75.0 \\ 75.0 \\ 75.0 \\ 75.0 \\ 75.0 \\ 75.0 \\ 75.0 \\ 75.0 \end{bmatrix} \text{, 31 in. span}$$

$$\lfloor \Pi \rceil = \lfloor 0.1666 \quad 0.5000 \quad 0.8333 \rceil \text{, 30 in. span}$$

$$\lfloor \Pi \rceil = \lfloor 0.1935 \quad 0.5161 \quad 0.8387 \rceil \text{, 31 in. span}$$

$$[I] = \begin{bmatrix} 0.08333 & 0.08333 & 0.08333 & 0.08333 & 0 & 0 & 0 & 0 & 0 & 0 & 0 & 0 \\ 0 & 0 & 0 & 0 & 0.08333 & 0.08333 & 0.08333 & 0.08333 & 0 & 0 & 0 & 0 \\ 0 & 0 & 0 & 0 & 0 & 0 & 0 & 0 & 0.08333 & 0.08333 & 0.08333 & 0.08333 \end{bmatrix} \text{, 30 in. span}$$

$$[I] = \begin{bmatrix} 0.08871 & 0.08871 & 0.08871 & 0.08871 & 0 & 0 & 0 & 0 & 0 & 0 & 0 & 0 \\ 0 & 0 & 0 & 0 & 0.08065 & 0.08065 & 0.08065 & 0.08065 & 0 & 0 & 0 & 0 \\ 0 & 0 & 0 & 0 & 0 & 0 & 0 & 0 & 0.08060 & 0.08060 & 0.08060 & 0.08060 \end{bmatrix} \text{, 31 in. span}$$

TABLE 4.2

THEORY TO TEST COMPARISONS, RECTANGULAR PLANFORM, ROOM TEMPERATURE

		$q = 4$ psi, $\{P_{Z_o}\}_1 = \{450, 300, 375\}$				$q = 6$ psi, $\{P_{Z_o}\}_1 = \{675, 450, 563\}$				$q = 8$ psi, $\{P_{Z_o}\}_3 = \{900, 600, 750\}$					
	Reference Points	Analysis I	Analysis II	Analysis III	Test	Analysis I	Analysis II	Analysis III	Test	Analysis I	Analysis II	Analysis III	IV	V	Test
$\{\alpha\}$	1	0.0308	0.0189	0.0287	0.0552	0.0385	0.0189	0.0297	0.0825	0.0322	0.0056	0.0010	0.0608	0.00397	0.1196
	2	0.0640	0.0614	0.0875	0.0637	0.1085	0.1025	0.1467	0.1096	0.1642	0.1508	0.2140	0.1365	0.18485	0.1818
	3	0.0551	0.0401	0.0665	0.0566	0.1005	0.0712	0.1120	0.1075	0.1660	0.1108	0.1890	0.0954	0.15365	0.1755
	4	0.0856	0.0795	0.1187	0.0993	0.1640	0.1500	0.2286	0.1900	0.2860	0.2500	0.3870	0.2176	0.31636	0.3146
	5	0.2500	0.2105	0.2498	0.2362	0.4170	0.3312	0.3950	0.4108	0.6160	0.4500	0.5230	0.3642	0.39375	0.6197
	6	0.2870	0.2671	0.3148	0.2875	0.4870	0.4527	0.5392	0.4700	0.7640	0.6750	0.8080	0.5765	0.64343	0.7923
	7	0.2660	0.2637	0.3192	0.2742	0.4880	0.4697	0.5774	0.4905	0.8050	0.7380	0.9170	0.6499	0.76285	0.8443
	8	0.2860	0.2946	0.3563	0.2814	0.5400	0.5419	0.6672	0.5125	0.9125	0.8820	1.1000	0.7859	0.92977	0.8763
	9	0.4210	0.4047	0.4582	0.4290	0.7240	0.6717	0.7687	0.7093	1.1180	0.9800	1.1210	0.7922	0.8334	1.1713
	10	0.4610	0.4503	0.5099	0.5215	0.8160	0.7723	0.8862	0.8610	1.2910	1.1680	1.3470	0.9818	1.0548	1.2818
	11	0.4380	0.4410	0.5064	0.4258	0.8000	0.7832	0.9134	0.7375	1.3160	1.2300	1.4440	1.0746	1.1942	1.2504
	12	0.4140	0.4270	0.4951	0.3952	0.7660	0.7733	0.9117	0.7229	1.2820	1.2400	1.4730	1.1125	1.2624	1.2246
$\{P_Z\}$	1	460	462	469	486	713	694	702	744	942	906	990	914	996	1001
	2	44	32	46	33	86	81	116	82	174	159	250	144	215	192
	3	15	11	17	15	40	28	47	42	88	59	11	50	89	74
	4	6	5	8	8	16	15	23	15	39	37	58	29	47	41
	5	427	407	428	420	774	706	756	760	1215	1070	1158	974	1007	1217
	6	98	94	112	99	262	243	292	252	560	491	591	416	468	577
	7	35	34	42	37	97	93	116	82	220	200	253	175	208	221
	8	10	10	12	9	28	29	36	22	69	66	86	58	70	64
	9	501	498	515	504	905	878	927	860	1480	1389	1490	1255	1281	1370
	10	91	88	101	103	252	237	276	267	565	503	593	413	448	561
	11	36	36	42	26	103	101	119	91	238	220	265	190	214	218
	12	12	13	15	10	38	39	47	34	97	93	117	81	95	85
C_{L_F}/C_{L_R}		1.54	1.50	1.59	1.56	1.96	1.96	2.02	1.93	2.53	2.30	2.60	2.09	2.196	2.50
Iterations, m - 0		6	6	6	-	7	8	9	-	10	10	17	For m = 0: Six minor $\{\alpha\}$ and $[\delta_{\alpha z}]$ loops, seven major $\{\alpha\}$ loops. Time ≈ 35 min. **Analysis IV and V**		
m - 1		25	-	-	-	NC	-	-	-	NC	NC	16			
Approx. machine Time, min, m - 0		0.45	0.46	0.50	-	0.53	0.55	0.58	-	0.60	0.60	1.50			

TABLE 4.3

THEORY TO TEST COMPARISONS, RECTANGULAR PLANFORM, ELEVATED TEMPERATURES

Thermal Test A — $\{\alpha\}$

Reference Points	$q = 4$ psi, $\{P_{Z_o}\}_1 = \{450, 300, 375\}$ Analysis VI	Analysis VII	Test	$q = 8$ psi, $\{P_{Z_o}\}_3 = \{900, 600, 750\}$ Analysis VI	Analysis VII	Test
1	0.0243	0.0283	0.0402	0.0221	0.0352	0.0967
2	0.0629	0.0617	0.0730	0.1700	0.1520	0.1887
3	0.0475	0.0858	0.0880	0.1461	0.2810	0.2440
4	0.0845	0.1204	0.1482	0.2890	0.4210	0.3973
5	0.2330	0.3121	0.2659	0.5580	0.8260	0.6781
6	0.2950	0.4040	0.3160	0.8280	1.2010	0.8313
7	0.2910	0.4112	0.3778	0.9010	1.3210	0.9905
8	0.3250	0.4610	0.3780	1.0670	1.5500	1.0911
9	0.4470	0.6880	0.5242	1.1910	2.0470	1.3585
10	0.5010	0.7520	0.5645	1.4390	2.3290	1.4627
11	0.4910	0.7250	0.5462	1.5130	2.3410	1.4483
12	0.4770	0.6780	0.5338	1.5270	2.2380	1.4520

Thermal Test B — $\{\alpha\}$

Reference Points	$q = 4$ psi, $\{P_{Z_o}\}_1 = \{450, 300, 375\}$ Analysis VI	Analysis VII	Test	$q = 8$ psi, $\{P_{Z_o}\}_3 = \{900, 600, 750\}$ Analysis VI	Analysis VII	Analysis VIII	Test
1	0.0248	0.0130	0.0775	0.0145	-0.0360	0.5540	0.1381
2	0.0668	0.0620	0.0740	0.1839	0.1280	0.1764	0.1689
3	0.0503	0.1540	0.1008	0.1610	0.5500	0.1038	0.2879
4	0.0916	0.1790	0.1865	0.3350	0.6750	0.3018	0.5128
5	0.2430	0.3930	0.3125	0.5900	1.1140	0.6905	0.6930
6	0.3120	0.5630	0.3692	0.9090	1.8180	1.0300	0.9299
7	0.3110	0.6050	0.4556	1.0100	2.1040	0.9632	1.2000
8	0.3500	0.6830	0.4977	1.2200	2.4800	1.0939	1.3679
9	0.4700	1.0360	0.5999	1.3000	3.4300	0.5218	1.5041
10	0.5320	1.1150	0.6614	1.6000	3.7900	1.3592	1.6898
11	0.5260	1.0670	0.6764	1.7000	3.7400	1.6697	1.7231
12	0.5130	0.9790	0.6501	1.7300	3.4900	1.6646	1.7557

Aeroelastic Analysis VIII: Solution type $m = 0$, seven minor $\{\alpha\}$ and $[\delta_{\alpha z}]$ loops, eight major $\{\alpha\}$ loops.
Approximate computer time 42 minutes.

SECTION 5.0
SUMMARY AND RECOMMENDATIONS

This report has formulated the governing mathematical relationships pertinent to nonlinear static aerothermoelastic behavior and has described the development of a method of solution for these equations as well as a related computer program for the purpose of obtaining such solutions. The method of solution for the equilibrium angles of attack is based on the iteration technique of Reference 16 and includes both nonlinear aerodynamic and nonlinear structural behavior. Completely new relationships for the flexural behavior of discrete elements were formulated in connection with the structural analysis portion of the solution method.

The present report has also described the development of a test technique for the simulation and measurement of static aeroelastic behavior in the presence of aerodynamic and structural nonlinearities and elevated temperatures. The system was successfully employed in the measurement of aeroelastic data under the cited conditions.

Analyses of test data were performed and, within the limitations of these analyses, theory-test comparisons were effected. Where structural nonlinearities did not play a role, or where such nonlinearities were of modest significance, it was found that the computer program is capable of furnishing results to an acceptable level of accuracy. The operational correctness of the program was thereby validated. Inadequacies in the formulation of the nonlinear terms of the structural analysis portion of the computer program were found, however. These appear to preclude the possibility of obtaining accurate predictions of deflectional behavior in the presence of severe structural nonlinearities with a feasible computational effort.

A critical examination of the results of this portion of the study discloses the following general deficiencies in the field of static aerothermoelastic analysis.

(1) The computational time required for an analysis of aerothermoelastic behavior which includes both structural and aerodynamic nonlinearities, is extremely long. With current digital computational capabilities (and if the techniques of iteration employed in this report are retained) the nonlinear aerothermoelastic analysis of a truly practical wing configuration would appear to be prohibitively expensive.

(2) Except for the results reported herein, which are limited in scope, there is no available information (in terms of planform reference point data) pertinent to nonlinear aerodynamic and structural behavior in combination. Thus, the complete range of validity of the solution procedures described herein cannot be ascertained and certain discrepancies made apparent by the test-theory comparisons of Section 4.0 cannot as yet be explained.

Based on these and other considerations the following specific recommendations are made:

(1) Additional experimentation, utilizing the experimental technique developed as part of the present study, should be conducted to obtain static aeroelastic data under both room and elevated temperatures. The specimens and test conditions should be designed to introduce nonlinear structural and aerodynamic behavior.

(2) The efficiency (i.e., speed) of the developed computer program should be improved through a study of the iterative solution processes, the convergence criteria and the improvement thereof.

(3) The accuracy and convergence characteristics of the developed computer program should be improved by the development of more satisfactory nonlinear terms in the discrete element force-displacement equations. (Present developments are detailed in Reference 17.)

(4) Additional test-theory comparisons, utilizing information and developments from items (1) to (3), should be accomplished.

It should also be noted that the study accomplishments have shown that new advances in important related areas are feasible. These include:

(1) The inclusion of inelastic behavior. Both creep and time-independent plastic flow can be of significance at elevated temperatures.

(2) The reorganization of the aeroelastic interaction computer program to permit independent analyses for nonlinear structural behavior.

SECTION 6.0

REFERENCES

1. Batt, J. R., Thermoelastic Effects on Hypersonic Stability and Control. Part I - "Hypersonic Aerodynamics" ASD TR 61-287, May 1963.

2. McClellan, C. H., Bertram, M. H., and Moore, J. A.,"An Investigation of Four Wings of Square Planform at a Mach Number of 6.9 in the Langley 11-Inch Hypersonic Tunnel,"NACA Report 1310, 1957.

3. Turner, M. J., Dill, E. H., Martin, H. C. and Melosh, R.,"Large Deflection of Structures Subjected to Heating and External Loads,"Journal of the Aerospace Sciences, V. 27, Feb. 1960.

4. Gallagher, R. H., Quinn, J. F., and Padlog, J.,"Deformational Response Determinations for Practical Heated Wing Structures,"Proc. of AIA-ONR Symposium on the Dynamics of High-Speed Flight, Los Angeles, California, April 1961.

5. Lansing, W., Jones, I., and Ratner, P.,"Non-Linear Analysis of Heated, Cambered Wings by the Matrix Force Method,"IAS Paper No. 62-107, June 1962.

6. Volsteen, L. and Fuller, R., "Behavior of a Cantilever Plate Under Rapid Heating Conditions," NACA RM L55E20c, 1955.

7. Batt, J. R., Nonlinear Thermoelastic Effects on Hypersonic Stability and Control, Part I, Volumes 1 and 2, FDL-TDR-64-16, January 1964, "Aerodynamics".

8. Padlog, J., and Gallagher, R. H., "Measurement of Angular Displacements of Practical Wing Structure by the Moire'-Fringe Technique," FDL-TDR-64-42, January 1964.

9. Diederich, F. W.,"A Simple Approximate Method for Calculating Spanwise Lift Distributions and Aerodynamic Influence Coefficients at Subsonic Speeds," NACA TN 2751, August 1952.

10. Zisfein, M. B., Donato, V. W., and Farrell, R. F., Supersonic Aeroelastic Effects on Static Stability and Control, Part I - "Aerodynamics" Volumes I and II, WADC TR 58-95, December 1958 (Confidential).

11. Batt, J. R., and Farrell, R. F., Thermal Effects on Static Aeroelastic Stability and Control, Part II - "Aerodynamics," Volumes I and II, WADC TR 58-378, December 1959 (Confidential).

12. Rattinger, I., and Gallagher, R. H., Supersonic Aeroelastic Effects on Static Stability and Control, Part III, "Structures" WADC TR 58-95, April 1960.

13. Gallagher, R. H., Quinn, J. F., and Turrentine, D., Thermal Effects on Static Aeroelastic Stability and Control, Part III, "Experimental and Analytical Methods for the Determination of Thermally-Affected Wing Deflectional Behavior", WADC TR 58-378, December 1959.

14. Gallagher, R. H., and Huff, R. D., Thermoelastic Effects on Hypersonic Stability and Control, Part II, Volume I, "Elastic Response Determination for Severely Heated Wings"; ASD TR 61-287, August 1962.

15. Huff, R. D., and Gallagher, R. H., Thermoelastic Effects on Hypersonic Stability and Control, Part II, Volume II, "Elastic Response Analysis of Fuselage and Combined Wing Fuselage Analysis."

16. Padlog, J., Donato, V. W., and Batt, J. R., Thermoelastic Effects on Hypersonic Stability and Control, "Hypersonic Aeroelasticity", ASD TR 61-287, Part III, May 1963.

17. "Computer Programs for the Solution of Nonlinear Static Aerothermoelastic Problems," — Available upon request, See Foreword.

18. Bennett, F. V.,"Comparison of Experimental and Theoretical Static Aeroelastic Loads and Deflections of a Thin 45° Delta Wing in Supersonic Flow," NACA TN D-974, October 1961.

19. Durgin, F. H., and Bartlett, C. J.,"A Measurement of the Static Aeroelastic Deformation and Loading of a Wing in Supersonic Flow,"ASD TDR 63-366, September 1963.

20. Dorrance, W.,"Two-Dimensional Airfoils at Moderate Hypersonic Speeds, Journal of the Aeronautical Sciences,"V. 19, Sept., 1952.

21. Ivey, H., Klunker, E., and Bowen, E.,"A Method for Determining the Aerodynamic Characteristics of Two-and Three-Dimensional Shapes at Hypersonic Speeds,"NACA TN 1613, July 1948.

22. Donato, V. W., Supersonic Aeroelastic Effects on Static Stability and Control, Part III, "Aeroelastic Interaction", WADC TR 58-95, July 1960.

23. Gallagher, R.H., Turrentine, D., and Quinn, J.F.,"Testing Techniques for Thermally Affected Complex Structures,"Experimental Mechanics, Aug. 1961.

24. Budiansky, B., and Mayers, J., "Influence of Aerodynamic Heating on the Effective Torsional Stiffness of Thin Wings," Journal of the Aeronautical Sciences, December 1956.

25. Turner, M.J., Clough, R., Martin, H.C., and Topp, L.J., "Stiffness and Deflection Analysis of Complex Structures," Journal of the Aeronautical Sciences, Volume 23, Number 9, Sept. 1956.

26. Gallagher, R.H., and Padlog, J., "A Discrete Element Approach to Structural Instability Analysis," AIAA Journal, Reader's Forum, June, 1963.

27. Gallagher, R.H., "A Correlation Study of Methods of Matrix Structural Analysis," AGARDograph 69, Pergamon Press, Oxford, 1964.

28. Gallagher, R.H., "Techniques for the Derivation of Element Stiffness Matrices," AIAA Journal, Vol. 1, June 1963.

29. Williams, D., "A General Method (Depending on the Aid of a Digital Computer) for Deriving Structural Influence Coefficients of Aeroplane Wings," RAE Report No. Structures 168, November 1954.

30. Gallagher, R.H., Padlog, J., and Huff, R.D., "Thermal Stress Determination Techniques for Supersonic Transport Aircraft Structures. Part III, Computer Programs for Beam, Plate, and Cylindrical Shell Analysis," ASD-TDR 63-783, Jan. 1964.